GRADUATE SCHOOL
EAST TENNESSEE STATE UNIVERSITY

East Tennessee State University
Digital Commons @ East Tennessee State University

Electronic Theses and Dissertations | Student Works

12-2021

Preparation and Study of Bacterial Membrane Models

Enoch Asimbisa
East Tennessee State University

Follow this and additional works at: https://dc.etsu.edu/etd

 Part of the Organic Chemistry Commons

Recommended Citation

Asimbisa, Enoch, "Preparation and Study of Bacterial Membrane Models" (2021). *Electronic Theses and Dissertations.* Paper 3995. https://dc.etsu.edu/etd/3995

This Thesis - unrestricted is brought to you for free and open access by the Student Works at Digital Commons @ East Tennessee State University. It has been accepted for inclusion in Electronic Theses and Dissertations by an authorized administrator of Digital Commons @ East Tennessee State University. For more information, please contact digilib@etsu.edu.

Preparation and Study of Bacterial Membrane Models

A thesis

presented to

the faculty of the Department of Chemistry

East Tennessee State University

In partial fulfillment

of the requirements for the degree

Master of Science in Chemistry

---

by

Enoch Agangloro Asimbisa

December 2021

Dr. Robert Standaert, Chair

Dr. Gregory W. Bishop

Dr. Abbas Gholipour Shilabin

Keywords: *Bacillus subtilis*, phospholipids, cell membrane, fluorescence, scattering, lignocellulosic feedstock

ABSTRACT

Preparation and Study of Bacterial Membrane Models

by

Enoch Agangloro Asimbisa

Fuel molecules are organic solvents that have disruptive effects on the bacterial membrane. This is a significant barrier in biofuel production, as it limits the fuel concentration that can be achieved through fermentation. One potential way of overcoming this barrier is to identify lipid compositions that can better withstand solvent stress, for which it is important to understand how organic solvents disrupt the membrane. Use of biophysical characterization techniques to quantify physical properties like fluidity and thickness will enable us to understand the mechanism by which solvents disrupt membranes. Native membranes are very complex, and we sought to develop *in-vitro* models for the membrane of the bacterium *Bacillus subtilis* that use pure phospholipids. Toward this goal, a number of the unusual *B. subtilis* fatty acids were synthesized, partial synthesis of the membrane phospholipids was achieved, and preliminary assessment of solvent effects on standard lipids was performed using a fluorescence technique.

DEDICATION

I dedicate this work to my family, friends, loved ones, and anybody who contributed to the success of this project.

ACKNOWLEDGMENTS

I thank God almighty, for the wisdom given me to embark on this project and for seeing me through successfully. I also would like to thank East Tennessee State University for the financial support, it meant a lot to me. My sincere gratitude to Dr. Robert Standaert, for his kind support and guidance through my entire research. I would also like to my family for their prayers and support.

My sincere gratitude to Dr. Abbas Shilabin and Dr. Gregory Bishop for accepting to be a part of my advisory committee and for their help on my thesis.

I would also like to thank Dr. Reza Mohseni for the instrumentation training given, it was helpful during my research work.

I am grateful to Maria Kalis and Haley Bell for their help in administrative and organizational aspects throughout my time in graduate school.

My earnest gratitude goes to my colleagues in Dr. Standaert lab, for their constant help and support during the entire research.

TABLE OF CONTENTS

LIST OF TABLES

LIST OF FIGURES

LIST OF ABBREVIATIONS

ATP	Adenosine triphosphate
CPS	Counts per second
CMC	Critical micelle concentration
ESR	Electron spin resonance
FA	Fatty acid
GC	Gas chromatography
GP	Generalized polarization
NMR	Nuclear magnetic resonance
PAF	Platelet activating factor
PC	Phosphatidylcholine
PE	Phosphatidylethanolamine
PG	Phosphatidylglycerol
PUFA	Polyunsaturated fatty acid
SANS	Small-angle neutron scattering
SAXS	Small angle X-ray scattering
THF	Tetrahydrofuran

CHAPTER 1. INTRODUCTION

Cell Membrane

The cell membrane, also known as the plasma membrane, is a protein-rich lipid bilayer that surrounds the cell and isolates the cytoplasm from its surrounding environment. Current models of the plasma membrane are simplified compositions of this highly complex cellular structure. Membrane models are used to appreciate basic membrane properties and membrane interactions with other biomolecules such as peptides, proteins, and drugs.[1]

The cell membrane is a critical and ubiquitous component of all cells. It performs many cellular functions such as molecular transport and communication, on top of the protection of the cell. It is quite interesting and not surprising that the targets for about 60% of drugs in most recent years are in membranes.[2,3] Eukaryotic cells (cells of higher organisms having cell nuclei) have multiple membrane-bound organelles in addition to the plasma membrane. These organelles, such as the endoplasmic reticulum, nucleus, mitochondrion, and Golgi apparatus, depicted in Figure 1,[4] perform specialized functions inside the cell. The plant cell has an extra protective layer known as the cell wall and chloroplasts for food manufacturing. These two features are the main differences between the plant cell and the animal cell.

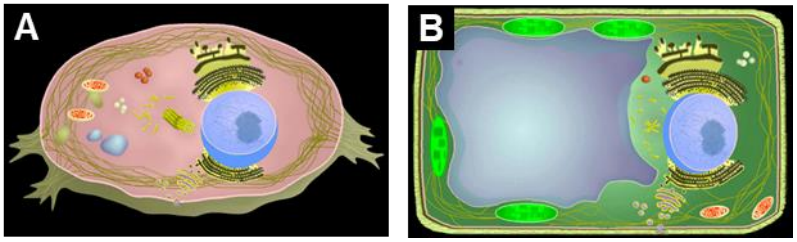

Figure 1. Eukaryotic cells (A) Animal cell and (B) plant cell. Copyright cellsalive.com, used with permission.

Fluid Mosaic Model

The fluid mosaic model is used to describe the structure of the cell membrane.[5] This model represents the membrane as a phospholipid bilayer in which phospholipid molecules and embedded proteins are free to move in any direction, hence, the membrane is fluid. The densely packed nature of the cell membrane makes it semi-permeable, preventing most substances from entering the cell. The membrane proteins provide functions such as recognition, signaling, and transport.

It is important to distinguish peripheral proteins from integral membrane proteins. Peripheral proteins are attached to the membrane through relatively weak interactions provided by, for example, a single fatty acid modification. Integral proteins comprise the majority of membrane proteins and have their polypeptide chains fully embedded in the membrane, often spanning it and having distinct intracellular and/or extracellular domains.

The membrane is in fact much richer in proteins,[6] and it is clear that integral proteins assume a significant role in membrane structure and integrity. The natural formation and function of the cell membrane rely on delicate interactions between the proteins and chemically compatible phospholipids. All of the interactions — lipid–lipid and lipid–protein — are potentially affected by biofuels and other solvent-like molecules.

Phospholipids

Phospholipids are the primary building blocks of the cell membrane.[7] Phospholipids are amphipathic, permitting them to self-assemble into a lipid bilayer when in an aqueous medium, as will be discussed below. Phospholipids are built on a backbone of *sn*-3-phosphoglycerol. The *sn*-1- and *sn*-2- positions are esterified with fatty acids (long-chain carboxylic acids, $\geq C_{12}$), providing hydrophobic tails to the molecule. The phosphoryl group may be free, making a

phosphatidic acid (PA), or esterified with any of several alcohols, forming the polar head to the molecule. Phospholipids comprising a major part of the plasma membrane include phosphatidylethanolamine (PE), phosphatidylcholine (PC), phosphatidylglycerol (PG), lysophosphatidic acid, and a dimeric form of PG, cardiolipin (CL) (Figure 2). Of these, bacterial membranes contain primarily PE and PG,[8,9] while mammalian membranes contain primarily PC and PE.

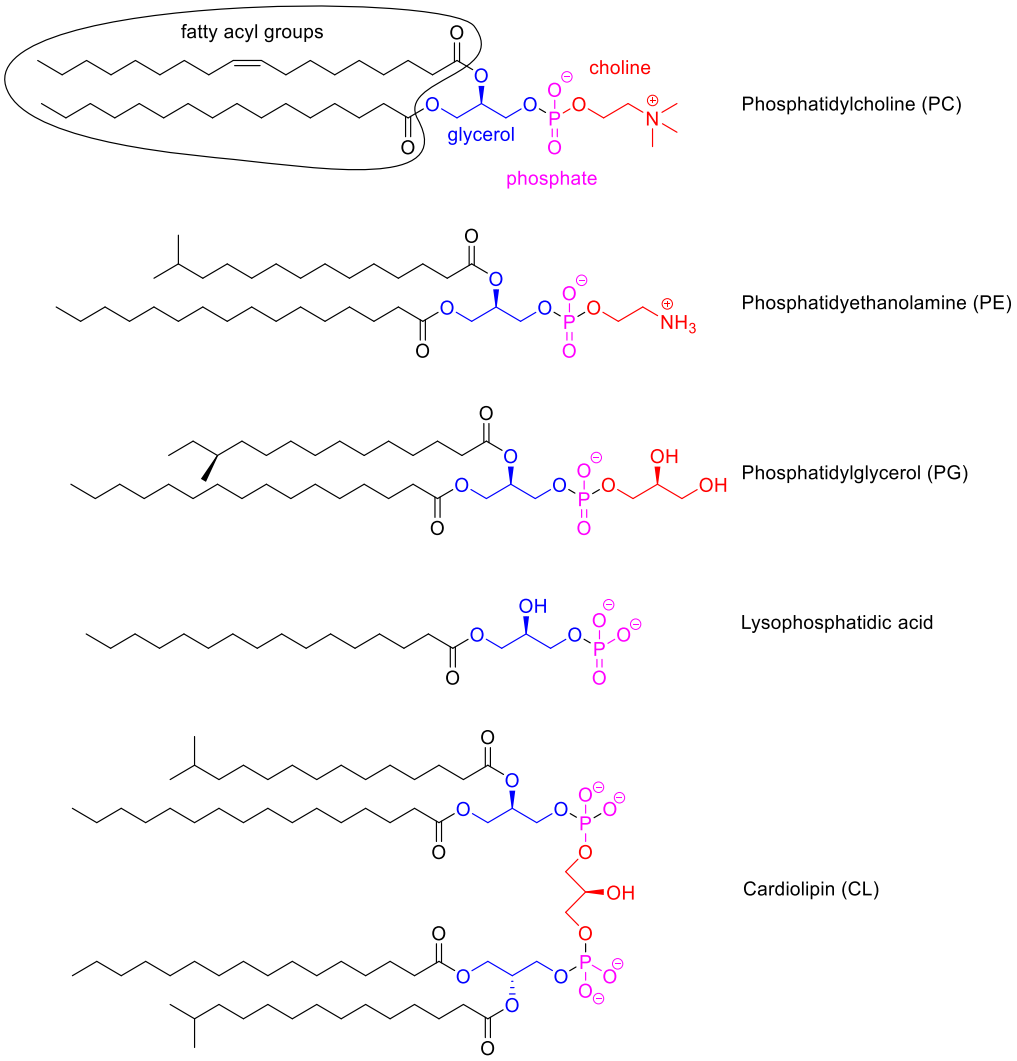

Figure 2. Chemical structures of phospholipids

The amphipathic structure of the polar membrane lipids drives self-assembly, such that there is a nonpolar environment in the heart of the bilayer for the hydrocarbon chains, with the lipid polar head groups confronting the aqueous medium, as shown in Figure 3. The opposing layers of the bilayers are called leaflets.

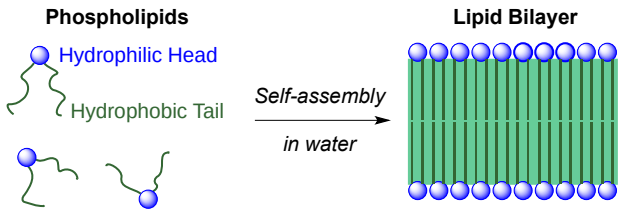

Figure 3. Self-assembly of phospholipids in water to form a lipid bilayer

In addition to phospholipids and proteins, membranes contain other important lipid modifiers. In mammalian cells, the most important one is cholesterol (Figure 4). Cholesterol's main role is to regulate fluidity and order of the bilayer,[6] preventing it both from gelling and thinning. It also forms specific interactions with other molecules. For example, it may regulate ion pumps, with some ion pumps relying exclusively on cholesterol to function.[6] Bacteria do not make cholesterol. Some species, such as *Escherichia coli*, make structurally related molecules called hopanoids.[6] The corresponding modifier in *B. subtilis* is unknown, though farnesyl alcohol is thought to play a role.[10] Our work anticipates model systems composed purely of phospholipids.

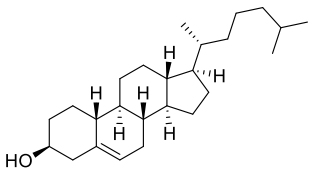

Figure 4. Structure of cholesterol

Fatty Acids

Generally, lipids comprise fatty acids (FAs) that are classified based on the presence or the absence of a double bond (saturated or unsaturated, respectively). FAs are carboxylic acids with a long hydrocarbon chain ($\geq C_{12}$). They are mostly found in phospholipid or triglyceride molecules (a glycerol backbone esterified to three fatty acids). A fatty acid is an essential source of metabolic fuel and energy storage because it produces a higher amount of adenosine triphosphate (ATP) when metabolized than does a sugar of the same weight.

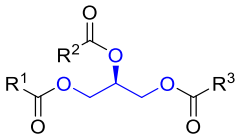

Figure 5. Generalized structure of triglycerides

Triglyceride molecules are hydrolyzed to form three fatty acids and a glycerol molecule. The use of a strong base such as sodium hydroxide (NaOH), produces glycerol and sodium salts of the fatty acids, a process called saponification, as shown in Figure 6.

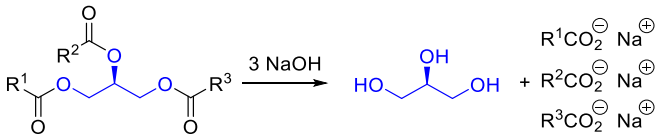

Figure 6. Saponification of triglycerides

The three main classes of fatty acids are polyunsaturated fatty acids (PUFAs), monounsaturated fatty acids (MUFAs), and saturated fatty acids (SFAs). SFAs are fatty acids without a carbon-carbon double bond. All cells use straight-chain (normal) fatty acids, notably the C_{14}-C_{18} even-chain fatty acids (Figure 7, left). These fatty acids are described in shorthand notation as 14:0, 16:0, and 18:0, indicating the number of carbons before the colon and the number of unsaturations after. Gram-positive bacteria such as *B. subtilis* use predominantly

branched-chain SFAs, with a single methyl branch at the penultimate carbon or the antepenultimate carbon in the chain referred to as iso-fatty acids and anteiso-fatty acids, respectively.[11] In phospholipids, branching inhibits close packing of the fatty acid tails, thereby lowering the melting point and maintaining a fluid phase. The predominant membrane fatty acids in *B. subitlis* are 16:0, i-14:0, a-15:0, i-15:0, i-16:0, a-17:0, and i-17:0, where the prefixes *a* and *i*, refer to anteiso and iso, respectively.[11]

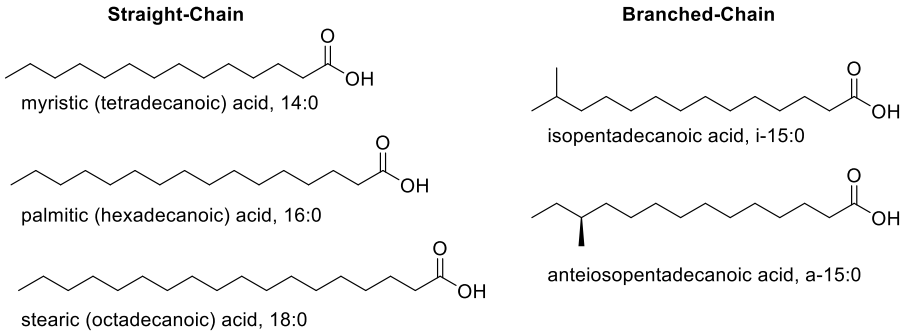

Figure 7. Chemical structures of common saturated fatty acids

Unsaturated fatty acids exist in either *cis* or *trans* configurations. The former configuration is common naturally, while the latter configuration is uncommon but can arise through heat, light, oxidation, and technological processes such as partial hydrogenation of unsaturated fatty acids. *Cis*-unsaturated fatty acids play an essential role in maintaining membrane fluidity, and they are also involved in vision, the secretion of inflammatory mediators, cell signaling, and regulation of lipid metabolism.[12] *Trans* configurations are not normally used by mammals. They pack tightly compared to *cis*-unsaturated lipids and reduce the fluidity of cell membranes.

Monounsaturated fatty acids (Figure 8) have just a single carbon-carbon double bond. Oleic acid, designated 18:1, is abundant in eukaryotic cell membranes and vegetable oils such as olive oil.

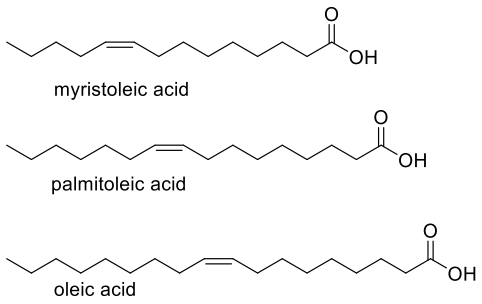

Figure 8. Chemical structures of monounsaturated fatty acids

Polyunsaturated fatty acids have two or more carbon-carbon double bonds, up to six double bonds (Figure 9). Current studies have shown a significant effect of PUFAs on human health. PUFAs are thought to help prevent diseases such as cancer, coronary heart disease, and cardiovascular disease.[13] Arachidonic acid, a tetra-unsaturated C_{20} PUFA, is the precursor for the biosynthesis of the prostaglandins, which help control muscular contraction and blood pressure.

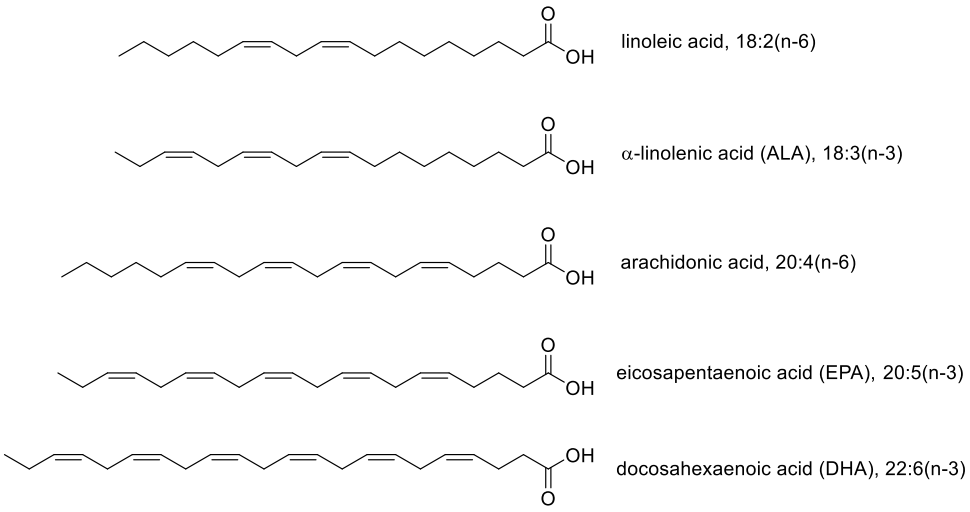

Figure 9. Chemical structures of polyunsaturated fatty acids. The parenthetical n-3 and n-6 descriptors identify the location of the double bond closest to the methyl terminus (n).

Mammals can synthesize monounsaturated fatty acids *de novo*, but not polyunsaturated fatty acids. Linoleic acid and α-linolenic acid are essential dietary nutrients. Mammals can convert these into longer PUFAs, but additional dietary intake is recommended. PUFAs are described by chain length and unsaturation, along with a descriptor identifying the location of the

double bond closest to the methyl terminus (designated *n*, or ω), commonly n-3 or n-6, with additional double bonds at three-carbon intervals.[14,15]

Membrane Fluidity

Cell membranes must maintain an optimal level of fluidity, achieved through a process called homeoviscous adaptation.[19] Membrane fluidity is determined by lipid packing, the thickness of the bilayer, and the rotational freedom that the lipids have in the bilayer. These, in turn, reflect chain length, branching, and unsaturation in the membrane fatty acids. Saturated lipids form relatively more ordered membranes (or more tightly packed membranes), with longer chains enhancing the effect.[22] Conversely, *cis*-unsaturated and branched lipids cannot pack tightly and form thinner, more disordered membranes, with more water penetration into the head and head-tail interface region.[16]

Studies with model membranes have shown that the thickness $2D_C$ of the hydrocarbon core for the common lipid POPC is 30 Å, whereas the overall (steric) thickness, D_B', is about 45 Å.[17,18] Selensky showed that the membrane lipids of *Esherichia coli* adapt to temperature stress to maintain a constant viscosity of about 2 poise (isolated lipids, no protein).[19] One major mechanism bacteria use for homeoviscous adaptation is altering their membrane fatty acid compositions.[20]

The easiest way to measure fluidity is with fluorescence spectroscopy. In 1979, a chemist named Gregorio Weber designed and synthesized an environmentally sensitive fluorescent dye, Laurdan, to study the dipolar relaxation phenomenon.[21,22] Laurdan has a 2-(dimethylamino)naphth-2-oyl chromophore (Figure 10) with a hydrophobic C_{11} side chain that inserts into lipid bilayers. Photoexcitation produces a large increase in dipole moment, which is

followed by reorientation of solvent dipoles. Polar solvents such as water stabilize the excited state, leading to a red-shift in the fluorescence emission.

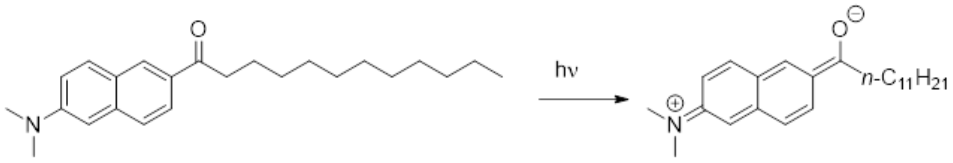

Figure 10. Structure of Laurdan (6-Dodecanoyl-*N*,*N*-dimethyl-2-naphthylamine). Photoexcitation of the chromophore produces a large increase in dipole moment.

Laurdan is one of the most used probes to measure fluidity and packing in biomembranes,[23,24,25] and its photophysical properties have been widely studied.[26,27,28] In lipid bilayers, two emission maxima are usually observed, at 440 nm and 490 nm. Emission at 440 nm is attributed to Laurdan in a more ordered region of the membrane, while emission at 490 nm is attributed to Laurdan in the least ordered, more water-exposed region. The relevant parameter for membrane studies is generalized polarization (GP), given by:

$$GP = \frac{I_{440} - I_{490}}{I_{440} + I_{490}}, \tag{1.1}$$

where I is the fluorescence emission intensity. The use of a polarity-sensitive probe is a straightforward way to deduce the membrane fluidity using simple fluorescence measurements.[29]

Harris and co-workers examined changes in membrane fluidity at different temperatures using Laurdan (GP) in dipalmitoyl phosphatidylcholine (DPPC) vesicles. They observed a significant phase transition from the more ordered gel phase to a less ordered liquid phase with a decrease in Laurdan GP values from 0.7 to −0.14 as temperature was increased from 20 to 50 °C.[30] Smith and coworkers also demonstrated using computational and scattering techniques that increasing concentrations of 1-butanol and THF resulted in an increase in membrane

fluidity, with 1-butanol having the stronger effect and targeting the head group–tail interface, while THF had a weaker effect and primarily targeted the tail region.[40]

Bacteria

Eukaryotic cells, as illustrated in Figure 1, have complex structures with multiple membrane-bound organelles, making it difficult to study individual membranes such as the plasma membrane. Bacteria are much simpler because they do not have membrane-bound organelles. There are two basic kinds of bacteria, Gram-positive and Gram-negative bacteria, as shown in Figure 11.[4] The distinction arose originally based on differences in histological staining properties, with Gram-positive bacteria staining with a stain used by Dr. Gram.[31] Subsequent work showed that Gram-negative bacteria like *E. coli* are surrounded by two membranes, inner and outer. However, Gram-positive bacteria have only one membrane. In this regard, they are ideal models for membrane research. Our research focuses on one Gram-positive model bacterium, *Bacillus subtilis*.

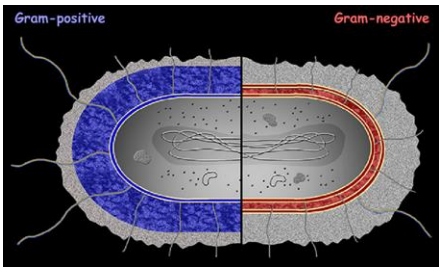

Figure 11. Structure of bacteria showing Gram-positive and Gram-negative types. Copyright cellsalive.com, used with permission

Bacillus subtilis

B. subtilis is found in soil, water, and the gastrointestinal tracts of animals such as cattle, goats, and sheep.[32,33] It has a natural ability to take up extracellular DNA, which facilitates

genetic modification.[34] In response to deprivation of nutrients and stress in the environment, *B. subtilis* forms highly resistant endospores, which are dormant and can survive various types of harsh conditions, such as very high temperatures and possibly even extraterrestrial conditions.[34] The spores are easily made airborne and dispersed by wind due to their light weight.[35,36]

Because of its safety and ease of genetic manipulation, *B. subtilis* has become the most important Gram-positive model organism. It is a workhorse that is used industrially in processes such as the production of insecticides, antibiotics, and fine biochemicals because of its diverse metabolism. It is also used as a pro-biotic, and its earliest use in food was the fermentation of soybeans to Natto, a Japanese traditional food.[37] It is also used extensively in research for the study of processes such as cell division, protein secretion, biofilm development, and many others.[19] The presence of a single membrane makes it ideal for our research.

B. subtilis has different lipids compared to mammalian cells. The two major differences are the fatty acid tail groups and the predominant phosphate head groups. As eukaryotes, mammals use straight-chain fatty acids with mixed saturated and unsaturated species to provide a fluid environment. In contrast, *B. subtilis* uses saturated lipids almost exclusively, with a mixture of straight and branched chains to control fluidity. In addition, *B. subtilis* and other bacteria use mostly PG and PE head groups, whereas mammalian cells use PC extensively in the plasma membrane, along with PE, PG, and other types.[38]

Biofuels

Biofuels are a renewable energy source, which are produced from organic materials. In addressing climate change concerns and the need for energy security, the United States government passed the Energy Security and Independence Act in 2007, setting a goal to create

thirty-six billion gallons of renewable fuel by 2022, with sixteen billion to be obtained from cellulosic ethanol-based fuels.[39] Within two years, great advances in the production of biofuels were seen. However, ethanol generated from starch remains the most-produced US biofuel, with 9 billion gallons generated in 2008.[39] The other major biofuel produced at present is biodiesel from palm, soybean, or rapeseed oil.

These biofuel feedstocks are energy-intensive, make incomplete use of the biomass, and require the use of food crops and farmlands. Given that neither ethanol nor biodiesel production can be scaled up enough to replace petroleum-derived transportation fuels, it is widely anticipated that biofuels of the future will likely be derived from agricultural waste or dedicated lignocellulosic energy crops such as switchgrass, corn stover, and poplar wood. Motives for the shift to lignocellulosic biomass as a feedstock are:[40]

- To avoid the use of food crops and farmlands.
- To make full use of biomass, not just the starch from corn or the sugar from sugar cane.
- To create better fuels than ethanol (second-generation candidates include 1-butanol).

This last point is important because the main biofuel produced, ethanol is less than ideal. The corrosivity and hygroscopic nature of ethanol make it unsuited for current fuel storage and distribution infrastructure. The construction of novel infrastructure for an ethanol economy would cost hundreds of billions of dollars.[39] Additionally, regardless of its high-octane number, ethanol has a low energy content, only 70% in comparison to gasoline. These shortcomings have instigated the need to create advanced biofuels that have higher energy content and are compatible with present transportation and storage infrastructure created for petroleum-based products. Improved biofuels need to have very similar properties to current transportation fuels.

Therefore, they must be compatible with existing distribution systems, storage infrastructure, and engines. A candidate second-generation biofuel is 1-butanol, which is superior to ethanol in important respects.[40]

The big problem with using lignocellulosic biomass generally is that, unlike starch and sugar, lignocellulose is refractory to fermentation. The sugars are in the form of insoluble polymers -- cellulose (glucose) and hemicellulose (xylan, a xylose polymer). In contrast, corn starch and sucrose are very soluble and easily fermented. Moreover, the polymeric sugars are also bound up by rigid, hydrophobic, and extensively cross-linked lignin (Figure 14).[41] Enzymes cannot get to the carbohydrate polymers to break them down into soluble, fermentable sugars.[41]

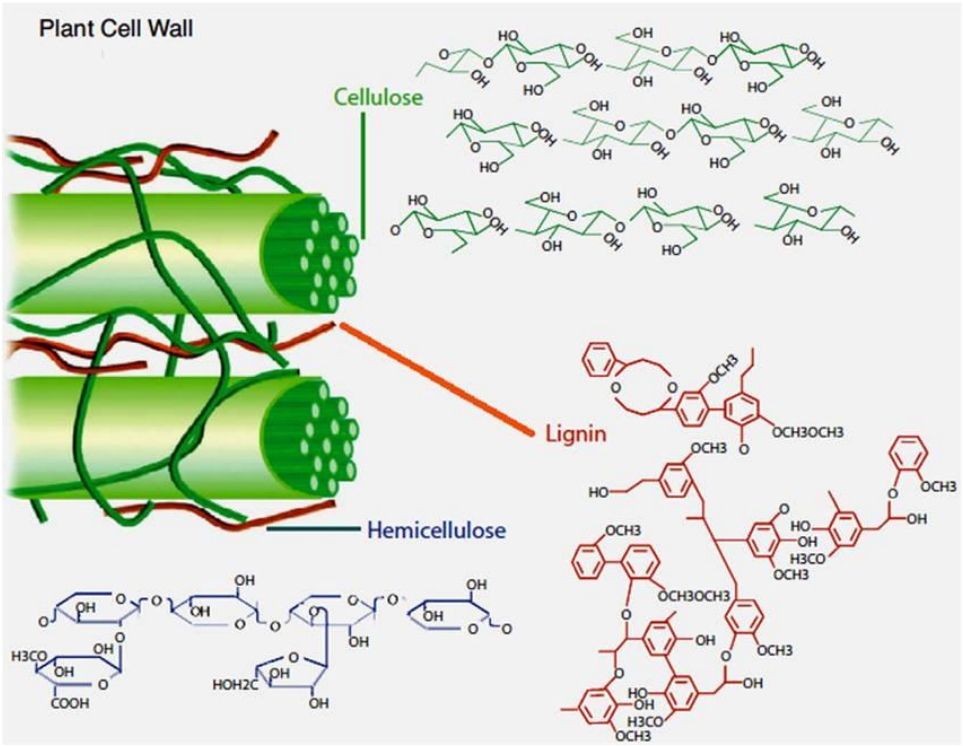

Figure 12. Structure of lignocellulose. Copyright Royal Society of Chemistry, reprinted with permission

For this reason, thermochemical pretreatment (e.g., ammonia/steam) is currently used to break down the structure physically and chemically to release fermentable sugars.[41] New

pretreatment technologies are under active investigation. One promising approach is to use organic co-solvents like tetrahydrofuran (THF) in water.[40]

In order for biofuels to compete economically with fossil fuels, the two processes of pretreatment and fermentation should work with the greatest possible volumetric productivity and atom economy. Biological catalysis, i.e., fermentation, is one possible solution to the challenge.[38,41] A major challenge in this context is the disruptive effect of the desired fuels and pretreatment solvents on the microbes used for fermentation. Biofuels are also organic solvents, and they are toxic to the producer organisms. The detrimental effects of organic solvents on whole cells hampers biotechnological processes such as biotransformation and environmental protection through bioremediation. The toxicity is due largely to the ability of the organic solvents to alter the cell membrane, leading to a change in the specific permeability.[42]

One potential way of overcoming this barrier is to identify lipid compositions or engineer microbes that can better withstand or resist solvent stress. For example, recent findings have detected a development of resistance to toxic solvents by bacteria such as some *Pseudomonas* strains. They develop resistance by altering the fatty acid composition, proteins, and phospholipid headgroups in their membranes.[38]

Going forward, it is important to understand at the molecular level how organic solvents disrupt the bacterial membrane. A recent paper explored this question through biophysical characterization of the membranes using scattering and fluorescence techniques accompanied by molecular dynamics simulations.[40] In this research, the effects of two organic solvents tetrahydrofuran (THF) and 1-butanol were examined. As discussed above, THF is employed in the pretreatment of lignocellulose to help break it down, and 1-butanol is a target biofuel. These two solvents would be encountered together in a bioprocess fermentation to produce 1-butanol.

Even though both THF and 1-butanol were found to partition into the microbial membrane, causing thinning and increased fluidity, the modes of interaction were different. Specifically, 1-butanol targeted the interface between the hydrophobic core of the membrane and the water-solvated head groups, whereas THF was distributed more uniformly throughout the membrane and partitioned into the tail region. My research will build on these findings by preparing models of the bacterial membrane and testing their solvent resistance.

Problem Statement

Successful processes for biofuel production are an economic and environmental priority. However, significant technological challenges remain. A fundamental problem is the toxicity of biofuels (especially second-generation biofuels like 1-butanol) and process solvents (like THF) to the microbes used for fermentation. Toxicity is a significant barrier in economical biofuel production, as it limits the fuel concentration that can be achieved. Understanding the mechanism of membrane toxicity, and identifying the most resistant membrane compositions, will help overcome this barrier. However, model lipids for important producer organisms are not commercially available. We seek to prepare suitable models and study the effect of fuels on membrane fluidity. Toward this goal, we initiated the synthesis of lipids from the bacterium *B. subtilis*, in particular phosphatidylglycerol (PG) lipids containing unusual branched fatty acids.

Goals

- To synthesize branched fatty acids used by *B. subtilis* and incorporate them into PG lipids.
- To prepare model membranes (unilamellar vesicles) from the synthetic lipids
- To study the fuel tolerance of the bacteria cell membrane as a function of lipid composition in model systems using Laurdan fluorescence as a probe of membrane fluidity.

CHAPTER 2. EXPERIMENTAL

Below (Table 1) is a list of chemicals and reagent used in this research.

Table 1. List of Chemicals Used

Name	Formula	Use	Supplier
Isopropylmagnesium chloride	C_3H_7ClMg	Reactant	Sigma Aldrich
sec-butylmagnesium chloride	C_4H_9ClMg	Reactant	Sigma Aldrich
Isobutylmagnesium chloride	C_4H_9ClMg	Reactant	Sigma Aldrich
2-Methylbutylmagnesium chloride	$C_5H_{11}ClMg$	Reactant	Sigma Aldrich
Di-*tert*-butyl-diisopropylphosphoramidite	$C_{14}H_{32}NO_2P$	Reactant	Sigma Aldrich
(*S*)- Glycidol	$C_3H_6O_2$	Reactant	Sigma Aldrich
Phosphorus oxychloride	PCl_3O	Reactant	Fisher
(*R*)-Solketal	$C_6H_{12}O_3$	Reactant	Sigma Aldrich
1H-Tetrazole	CH_2N_4	Reactant	Alpha Aesar
Lithium tetrachlorocuprate	Li_2CuCl_4	Catalyst	Sigma Aldrich
Triethylamine	$C_6H_{15}N$	TLC	Alpha Aesar
Thionyl chloride	$SOCl_2$	Reactant	Alpha Aesar
Tetrahydrofuran	C_4H_8O	Dissolve	Alpha Aesar
Silica gel	SiO_2	Filtration	Silicyde
Cesium carbonate	Cs_2CO_3	Reactant	Alpha Aesar
Choline tosylate	$C_{12}H_{21}NO_4S$	Reactant	Lab-made
4-Dimethylaminopyridine (DMAP)	$C_7H_{10}N_2$	Reactant	Acros Organics
Chloroform	$CHCl_3$	Solvent	Various
Glacial acetic acid	$C_2H_4O_2$	Reactant	Fischer
Acetone	C_3H_6O	Solvent	Fischer
Methanol (dry)	CH_3OH	Solvent	Fischer
Trichloroacetonitrile	C_2Cl_3N	Reactant	Acros Organics
Ether	$C_4H_{10}O$	Solvent	Fisher
Toluene	C_7H_8	Solvent	Fisher

Gas Chromatography/Mass Spectrometry (GC/MS) Analysis

GC/MS analysis was performed on a Shimadzu GC-2010 gas chromatograph equipped with an AOC-20i autosampler, an SHRXI-5MS capillary column (length 30 m, inside diameter 0.25 mm, film thickness 0.25 μm) and a GCMS-QP2010 mass-sensitive detector operating in electron impact mode at 70 eV.

Analyses were performed using He carrier gas at a flow rate of 1 mL/min, an inlet temperature of 260 ℃, an ion-source temperature of 200 ℃, and a transfer line temperature of 250 ℃. The initial oven temperature of 50 ℃ was held for 2 min, ramped at 20 ℃/min to 280 ℃, and held for 2 min. An injection volume of 1 μL and a split ratio of 20:1 were used.

Fatty acids were converted to their methyl esters (FAMEs) for GC/MS analysis. In a typical procedure, a small portion (0.1–1 mg) m of the fatty acid (or the equivalent amount of reaction mixture) was placed into a 13×100-mm screw-cap test tube. A fresh (<30 days old) solution of 10% concentrated HCl in methanol was added, and the tube was sealed followed by heating at 85 ℃ for 2 h. The solution was allowed to cool to room temperature, followed by the addition of 1.0 mL hexane and 1.0 mL of deionized water. The sample was vortex-mixed and allowed to separate into two phases. The upper (hexane) layer was transferred into a 2 mL autosampler vial and diluted to a volume of 1 mL for analysis.

Synthesis of Fatty Acids

B. subtilis branched-chain fatty acids were synthesized using the method of Baer and Carney.[43] The synthesis of 12-methyltridecanoic acid (isotetradecanoic acid, i-14:0) from 11-bromoundecanoic acid and isopropylmagnesium chloride is presented as an illustrative example. Other fatty acids were synthesized analogously.

A pre-weighed, 50-mL round bottom flask with a magnetic stirring bar was heated and flushed with nitrogen gas to remove moisture. A portion of solid 11-bromoundecanoic acid (2.01 g, 7.58 mmol) was introduced into the flask, which was then sealed with a septum and flushed with nitrogen gas. THF (9.4 mL) was added to dissolve the sample, and the solution was cooled with stirring in an isopropyl alcohol/dry ice bath maintained at −20 °C. Isopropyl magnesium chloride solution (3.8 mL, 2.0 M in THF, 7.6 mmol, 1.0 equiv) was cautiously added dropwise while maintaining the bath temperature at −20 °C to deprotonate the carboxylic acid. Lithium tetrachlorocuprate (1.5 mL, 0.10 M in THF, 0.15 mmol, 0.02 equiv) was added, followed by dropwise introduction of an additional portion of isopropyl magnesium chloride solution (4.0 mL, 8.0 mmol, 1.05 equiv). The sealed reaction flask was then kept in a −20 °C freezer overnight. To verify completion of the reaction, an aliquot (1 μL) of the reaction mixture was withdrawn and subjected to fatty acid methyl ester (FAME) GC/MS analysis as described below. Additional portions of isopropylmagnesium chloride were introduced, followed by incubation periods of at least 4 h, until the reaction was judged complete by FAME GC/MS analysis.

The reaction mixture was allowed to warm to room temperature and was transferred with the aid of 50 mL of toluene to a separatory funnel, and sulfuric acid (1.0 M, 25 mL) was cautiously added. After extraction, the blue aqueous phase was removed, and the organic phase was extracted with 0.1 M H_2SO_4, then filtered to remove solids. To remove residual copper, the solution was extracted with a solution of 45 mg of Na_2S in water and filtered again. After the solution was dried over sodium sulfate, filtered and concentrated by rotary evaporation, the product was purified by Kugelrohr distillation under vacuum (< 1 mm Hg), affording 1.51 g (7.05 mmol, 87.0 %) of the product as a white solid. ^{1}H NMR (400 MHz, $CDCl_3$) δ (ppm) 0.85

(6H, d, *J*=6.60 Hz), 1.16-1.08 (2H, m), 1.44-1.18 (14H, m), 1.50 (2H, non, *J*=6.6 Hz), 1.61 (2H, br p, *J*=7.0 Hz), 2.33 (2H, t, *J*=7.5 Hz), 11.2 (1H, br s)

Synthesis of 12-Bromodecanoic Acid

The procedure followed that reported by Bidd et al.[44] In a 50-mL round bottom flask, acetic anhydride (5.0 mL) was carefully added to 8.0 mL of hydrobromic acid, which was followed by the addition of 12-hydroxydodecanoic acid (4.0 g, 0.018 mmol). The mixture was refluxed for 3 h, allowed to cool down to room temperature and concentrated to obtain a brown solid. The residue was then recrystallized from hexane to obtain crude 12-bromododecanoic acid as white, fine crystals. ^{1}H NMR (400 MHz, $CDCl_3$) δ (ppm) 1.25 (br m, 12H), 1.40 (br p, 2H, *J*= 7.0 Hz), 1.61 (p, 2H, *J* = 7.3 Hz), 1.83 (p, 2H *J*= 7.2 Hz), 2.33 (t, 2H, *J* = 7.6 Hz), 3.39 (t, 2H, *J* = 7.0 Hz), 9.2 (br s, 1H); MS(EI): *m/z* 352 (1%, M+2), 350 (1, M), 335/337 (3/3, M−CH_3), 271 (12, M−Br), 132 (61, ($C_5H_{12}O_2Si$), 117 (100, $C_4H_9O_2Si$).

Synthesis of 3-O-(Di-O-tert-Butylphosphono)-1-O-Palmitoyl-sn-Glycerol

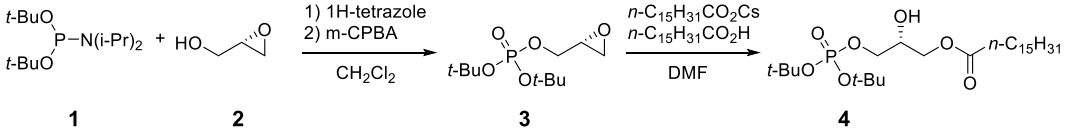

Figure 13. General scheme for synthesis of (*R*)-*O*-(di-*tert*-butylphosphono)glycidol

The procedure was essentially as described by Lindberg et al.[45] First, to synthesize (*R*)-*O*-(di-*tert*-butylphosphono)glycidol (3), 1H-tetrazole in acetonitrile solution (0.40 M, 9.4 mL, 4.2 mmol) was cautiously added to a stirred solution of (*S*)-glycidol (**2**, 238 mg, 3.21 mmol) and di-*tert*-butyl-*N*,*N*-diisopropyl phosphoramidite (**1**, 1.58 g, 5.70 mmol) in 100 mL of dichloromethane. The solution was stirred for 30 min, then cooled to 0 °C. *m*-CPBA (77% purity, 1.70 g, 9.85 mmol) was added to the mixture and stirred for 40 min. The reaction was quenched

with 10% aqueous $Na_2S_2O_3$, washed with saturated $NaHCO_3$, dried over anhydrous sodium sulfate, filtered, and concentrated. Flash chromatography using hexane:ethyl acetate; 2:1, 1:1, and finally 1:1.5 containing 0.1% triethylamine (NEt_3) was carried out to obtain the pure compound. ^{1}H NMR data matched those reported by Lindberg et al.

Cesium palmitate was synthesized according to a modification of the approach reported by Wim et al.[46] Cesium carbonate (325 mg, 1.00 mmol) was dissolved in 10 mL of methanol (CH_3OH) and heated to 40 ^oC. Palmitic acid (770 mg, 3.00 mmol) was added in portions while stirring. Excess palmitic acid is needed to ensure a complete reaction. The mixture was allowed to cool to room temperature, and the methanol was removed on the rotary evaporator. The product was suspended in 50 mL of ether to dissolve the excess palmitic acid, collected by filtration and washed thoroughly with ether and dried in vacuo, affording 325 mg (67 %) of cesium palmitate as a white solid.

3-*O*-(Di-*O*-*tert*-butylphosphono)-1-*O*-palmitoyl-*sn*-glycerol (4). The procedure was a slight modification of the one reported by Lindberg et al.[45] A mixture of epoxide **3** (52.0 mg, 0.197 mmol), palmitic acid (50.0 mg, 0.197 mmol, 1.0 equiv) , and cesium palmitate (228 mg, 0.585 mmol 3.0 equiv) in DMF (2.1 mL) was stirred while heating at 80 °C in an oil bath for 10 h, and the mixture was allowed to cool to room temperature. To the mixture was added 45 mL of toluene, and the solvents were evaporated to obtain a white powder. Chloroform was added to the mixture, suspended solids were removed by filtration, and the solvent was evaporated under a stream of nitrogen.^{1}H NMR data matched those reported by Lindberg et al.

Membrane Fluidity Studies

Laurdan was incorporated at 0.5 mole percent into phosphatidylglycerol (POPG) via dry films, which were hydrated and extruded into 100-nm large unilamellar vesicles (LUVs). A stock solution of Laurdan was prepared by dissolving approximately 5 mg of Laurdan in 12 mL of methanol. This solution was further diluted tenfold with methanol to give a working Laurdan stock, the concentration of which was determined to be 93 μM by UV spectroscopic analysis using molar absorptivity (ε_{364}) = 20,000 $M^{-1}cm^{-1}$.[47] Quantitation was performed using a sample of the working stock that had been diluted with an equal volume of methanol to reduce A_{364} below 1.

Solutions of 1-palmitoyl-2-oleoyl-*sn*-glycero-3-phospho-(1'-*rac*-glycerol) (POPG) in chloroform (0.50 mL, 10 mg/mL 13.0 mM, 6.5 μmol) and 93-μM Laurdan in methanol (0.35 mL, 33 nmol, 0.5 mol %) were mixed and evaporated to dryness under a stream of nitrogen. The dried sample was redissolved in 2.0 mL of chloroform, then re-evaporated ~~t~~o aid in removing traces of methanol and finally placed *in vacuo* (< 1 mm Hg) for at least 2 h to remove traces of volatiles. Rehydration was performed by adding 1.0 mL of deionized water, followed by vortex mixing. The sample was kept in a water bath at a temperature of 50 ℃ with intermittent vortexing for 2 mins. to obtain a slightly cloudy suspension. The solution was then subjected to five freeze-thaw cycles by freezing on dry ice followed by heating and vortexing at 50 ℃ for 2 min. Finally, the suspension was extruded by 31 passages through a 100-nm pore-size membrane using an Avanti manual extruder at a temperature of 40 ℃.

Fluorescence spectra at various temperatures were then recorded on a Horiba Fluoro-Max 3 spectrofluorometer with an excitation wavelength of 350 nm, and GP was calculated according to Eq. 1.1.

CHAPTER 3. RESULTS AND DISCUSSION

Our research is aimed at generating lipid models of the *B. subtilis* membrane for the study of biofuel stress using Laurdan general polarization. Bacterial model lipids (PE and PG) and chimeric lipids containing the mammalian head group phosphatidylglycerol (PC), which are not commercially available, are required for this research. While synthesis of a library of PE, PG, and PC lipids will be necessary for comprehensive study of biofuel stress on model membranes, the focus of this thesis work is on the synthesis and characterization of PG lipids containing branched fatty acids common in *B. subtilis*.

Synthesis of Fatty Acids

The synthesis of fatty acids relied on a copper-catalyzed Grignard reaction as described by Baer and Carney.[43] As a representative example, 12-methyltridecanoic acid (i-14:0) was synthesized using 11-bromododecanoic acid and isobutyl magnesium chloride in the presence of lithium tetrachlorocuprate at low temperature (−20 °C). The first equivalent of Grignard reagent is consumed in an acid-base reaction, producing a carboxylate salt, and the second equivalent undergoes copper catalyzed coupling where the bromine is substituted by the isobutyl group from the Grignard reagent (Figure 17). Reaction progress was monitored by GC/MS using small aliquots from the reaction mixture, and additional Grignard reagent was added as needed to assure complete consumption of the bromide. After workup and Kugelrohr vacuum distillation, the purity of the product was confirmed by GC/MS (Figure 16).

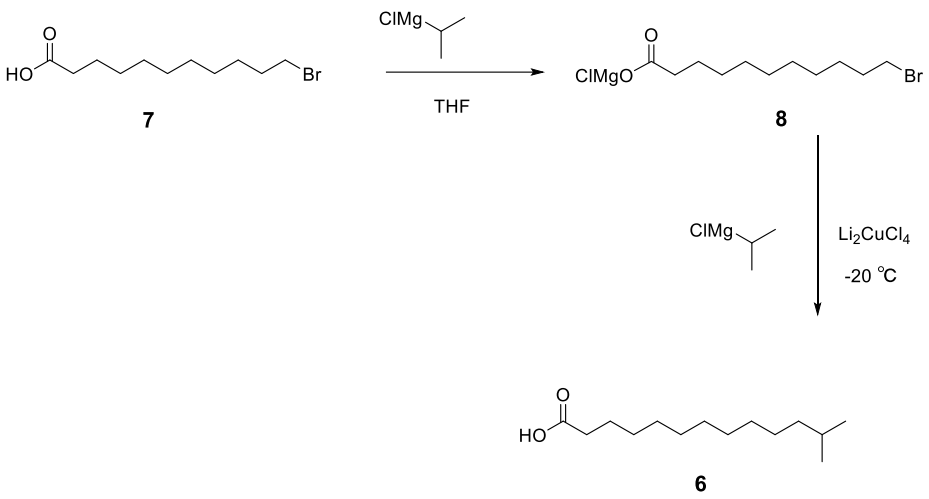

Figure 14. Synthesis of fatty acids by copper-catalyzed Grignard coupling

For GC/MS analysis, fatty acids were first converted into their methyl esters (FAMEs, Figure 17), which are more volatile, less polar and better-behaved in GC. This process was carried out at 85 °C in a 10% (v/v) solution of concentrated HCl in methanol. The conversion is through a process known as Fischer esterification, where the hydroxy group of the fatty acid is replaced by an alkoxy group in the presence of an acid catalyst.

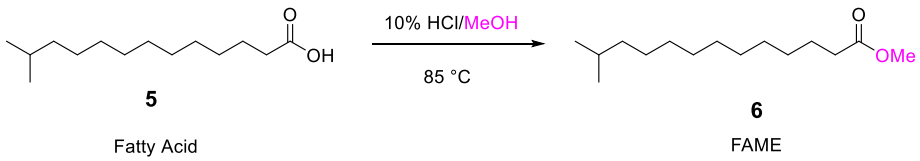

Figure 15. Fatty acid methyl ester (FAME) derivatization

The GC/MS total ion chromatogram for **6** is shown in Figure 18. The mass spectrum (Figure 19) for the species with retention time of 10.684 min showed a molecular ion at *m/z* 242 (0.2%), along with a base peak at *m/z* 74 corresponding to the $[CH_3OC(OH)C=CH_2]^+$ fragment produced via the McClafferty rearrangement (Figure 20). Additional expected fragments at 227

($M-CH_3$), 211 ($M-OCH_3$), and 199 ($M-C_3H_7$) were also observed.

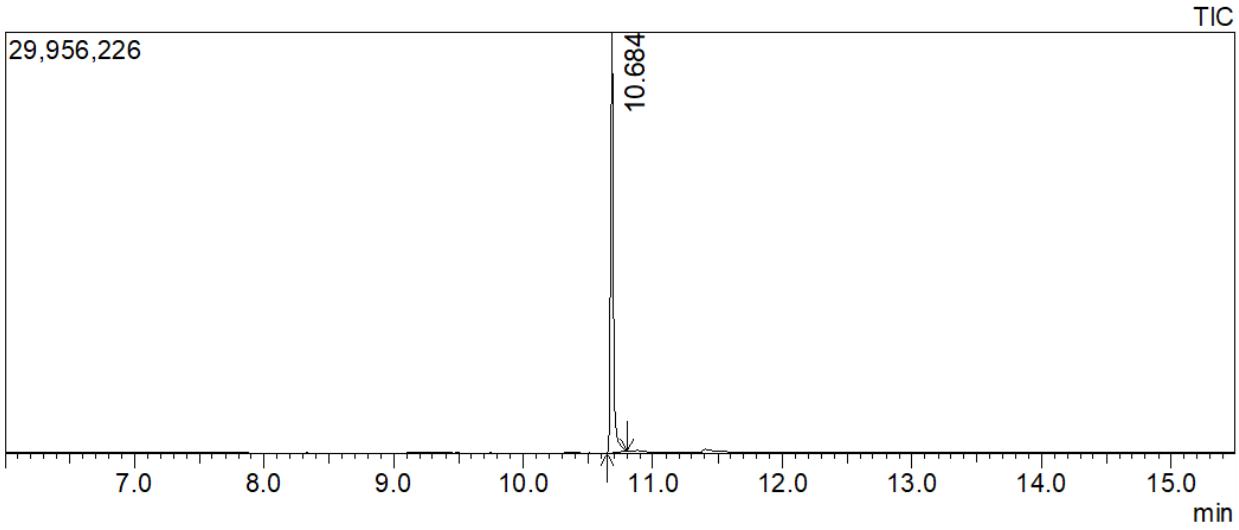

Figure 16. GC/MS Total ion chromatogram of 12-methyltridecanoic acid (i-14:0) methyl ester (**6**)

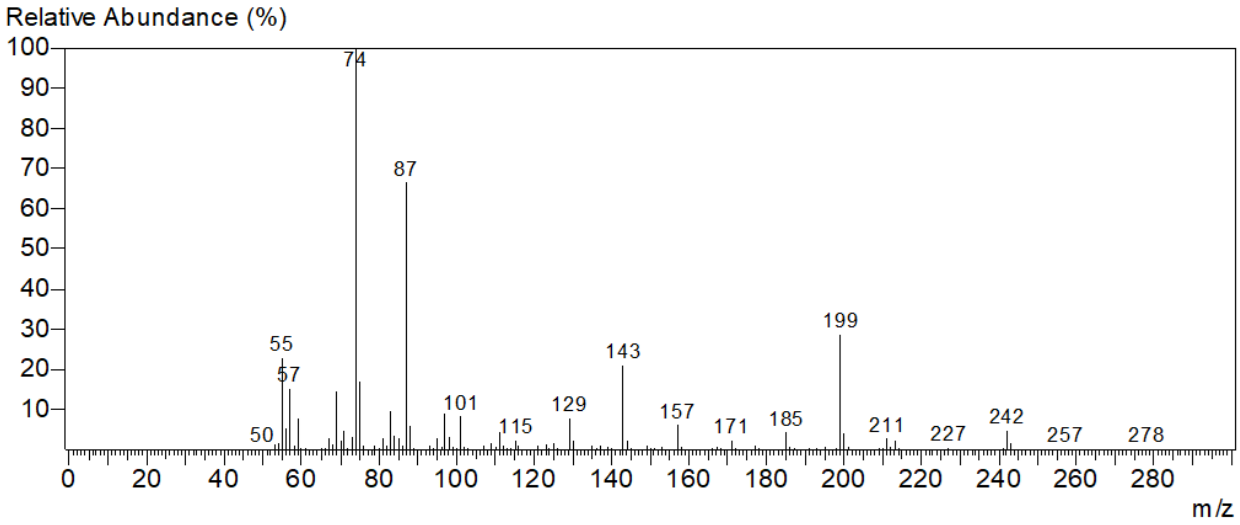

Figure 17. Electron-impact mass spectrum of 12-methyltridecanoic acid (i-14:0) methyl ester (**6**) (M+ = *m/z* 242)

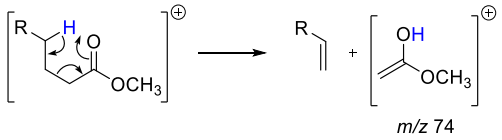

Figure 18. McClafferty rearrangement

In the same way, four other fatty acids were synthesized from 11-bromoundecanoic acid and commercially available Grignard reagents by my colleagues in Dr. Standaert's laboratory. From Figure 18 and Table 2 below, it is observed that each gas chromatogram showed a single major peak that represents the expected product with retention times between 10.70 and 11.81 min for each methyl ester derivative. The retention times are consistent with the expectation that shorter and more volatile FAMEs will elute earlier. For example, 12-methyltridecanoic acid methyl ester has a shorter retention time (10.70 min) than 13-methylpentadecanoic methyl ester (11.81 min). Yields obtained were between 21% and 87%, which is comparable to the 40–94% reported by Baer and Carney. The lower yields in our synthesized fatty acids usually resulted from losses during isolation and purification. Identification of each fatty acid methyl ester was accomplished by analysis of its mass spectrum and comparison with the library standard spectrum.

Table 2. Fatty Acid Methyl Esters with Their Respective Retention Times

Grignard Reagent	Mass of 7 (g)	Product	Yield (g)	Yield (%)	Retention time (min)
i-PrMgCl	2.006	12-methyltridecanoic acid (i-14:0)	1.510	87	10.684
i-BuMgCl	2.045	13-methyltetradecanoic acid (i-15:0)	1.020	55	11.273
s-BuMgCl	2.014	12-methyltetradecanoic acid (a-15:0)	0.909	49	11.306
i-C_5H_{11}MgCl	2.000	14-methylpentadecanoic acid (i-16:0)	1.210	62	11.777
2-methylbutyl MgCl	2.009	13-methylpentadecanoic acid (a-16:0)	0.40	21	11.811

^{1}H NMR spectra recorded at 400 MHz in $CDCl_3$ were also used for the characterization and identification of the synthesized fatty acids. The ^{1}H NMR spectrum of i-14:0 (Figure 21) shows peaks that indicate the presence of the desired compound. However, additional peaks, particularly a triplet at δ 3.4 and 1.6 ppm, were not consistent with the product and represent an impurity that was not evident from GC/MS, at an estimated level of about 10% based on ^{1}H NMR integration. The impurity resonances are consistent with the bromo-acid starting material. Additional purification or resynthesis is required, but because of the delay between synthesis and availability of the NMR spectrometer, time did not permit additional effort on the compound.

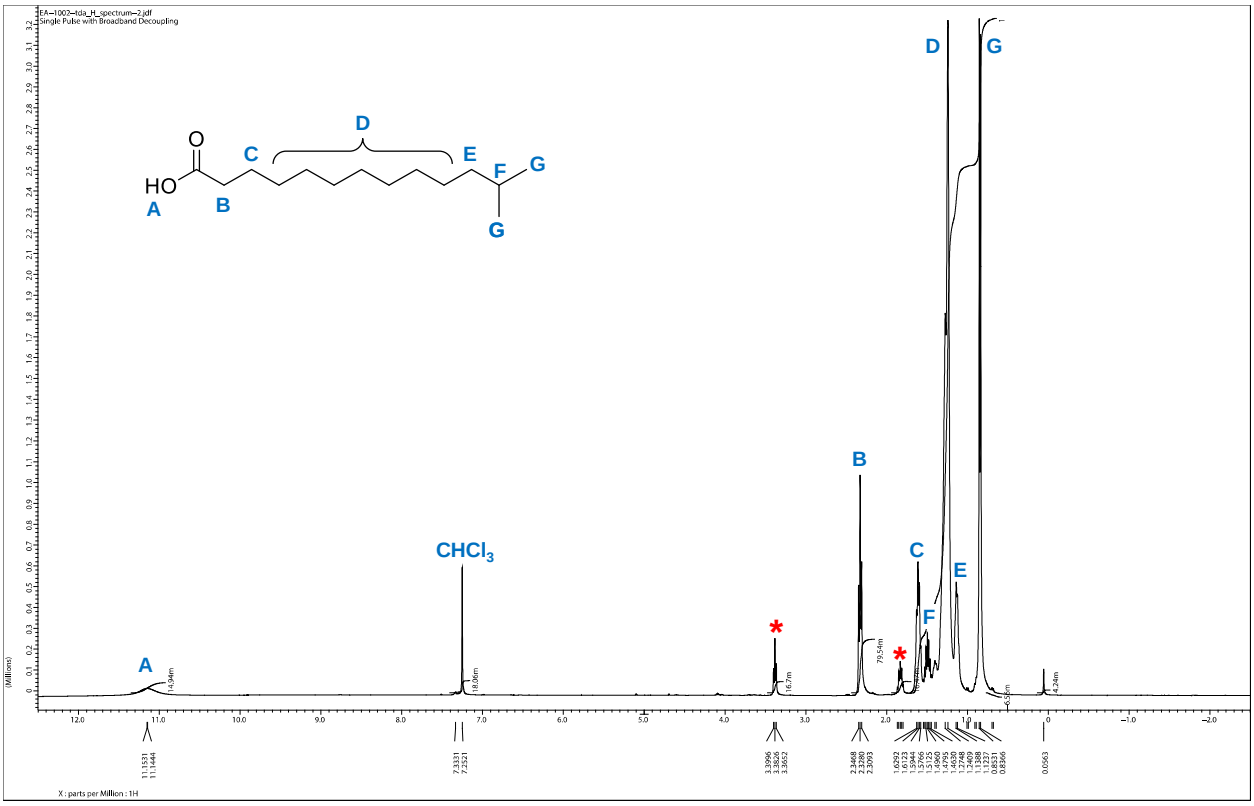

Figure 19. ^{1}H NMR Spectrum of 12-methyltridecanoic acid (i-14:0) **(6)**. Impurity peaks at δ 3.4 and 1.9 are marked with *.

As a precursor to longer-chain fatty acids, 12-bromododecanoic acid was synthesized from the corresponding hydroxyacid with HBr and acetic anhydride (Figure 22). GC analysis of the 12-bromododecanoic acid as its FAME derivative showed the expected product at a retention time of 11.89 min (Figure 23). In the mass spectrum (Figure 24) of the species with this retention time, a weak molecular ion was observed, with peaks of equal intensity at m/z 292 and 294 reflecting the equal abundance of ^{79}Br and ^{81}Br, along with expected fragments at 261/263 (loss of CH_3O) and 213 (loss of Br). A significant impurity peak representing approximately 35% of the product was observed at a retention time of 11.37 (Figure 22). The mass spectrum of this compound (Figure 25) was very similar to that of the expected product but lacked the molecular ion. Critical examination of the spectrum led to the identification of this impurity as 12-chlorododecanoic acid, produced as an artifact of derivatization through S_N2 substitution of

chloride (from HCl) for bromide. The mass spectrum similarly displayed weak molecular ion peaks at *m/z* 248 and 250 with intensities in the characteristic 3:1 ratio of ^{35}Cl to ^{37}Cl, and similar fragment ions at *m/z* 217/219 (loss of CH_3O) and *m/z* 213 (loss of Cl). The shorter retention time of the chloro-derivative is consistent with expectation based on its lower molecular weight.

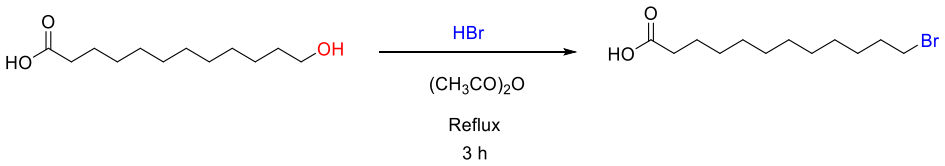

Figure 20. Synthesis of 12-bromododecanoic acid

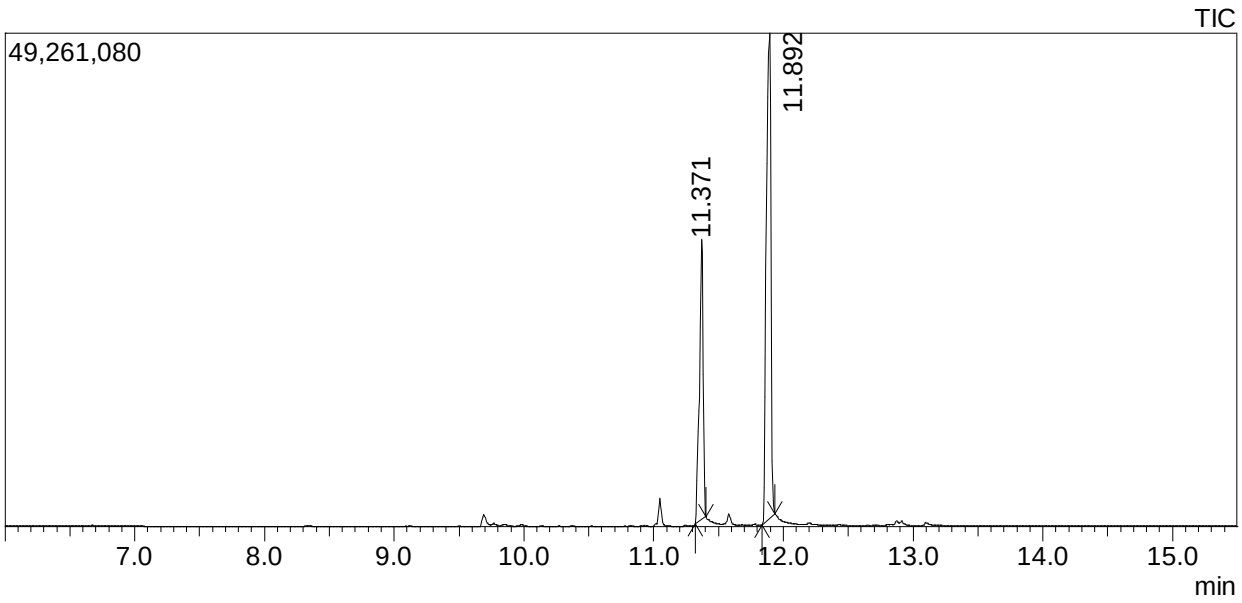

Figure 21. GC/MS total ion chromatogram of 12-bromododecanoic acid methyl ester. The product elutes at 11.982 min, whereas the corresponding 12-chloroester, formed as an artifact of esterification in HCl/methanol, elutes at 11.371 min.

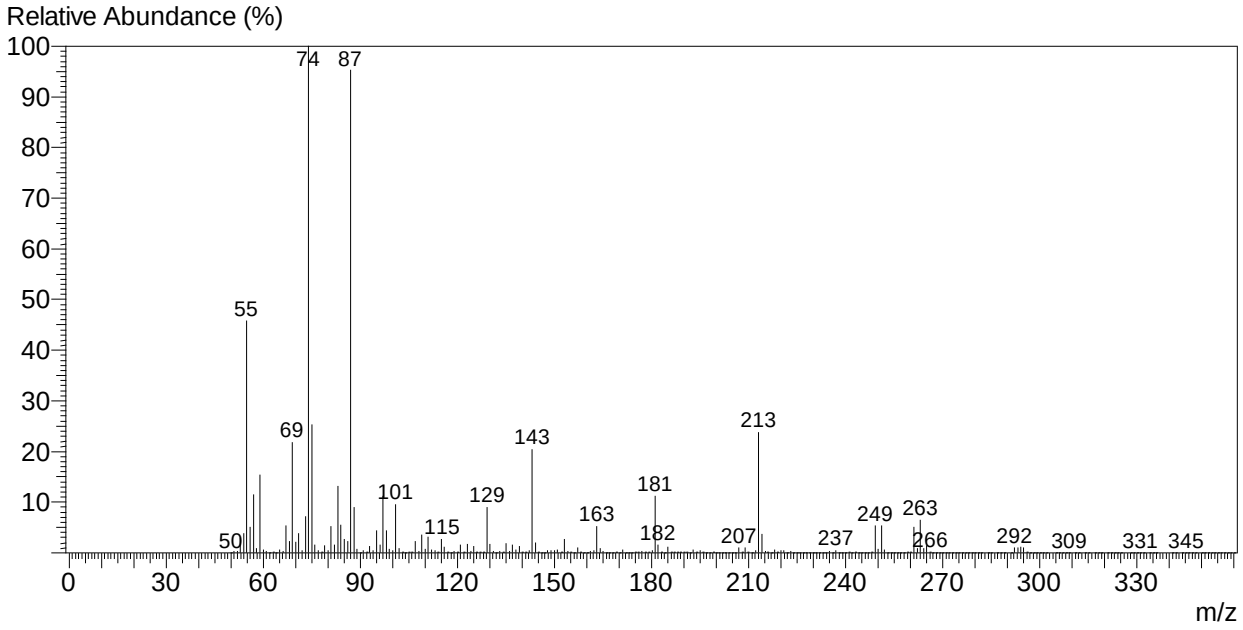

Figure 22. Electron-impact mass spectrum of 12-bromododecanoic acid methyl ester (M+ = *m/z* 292)

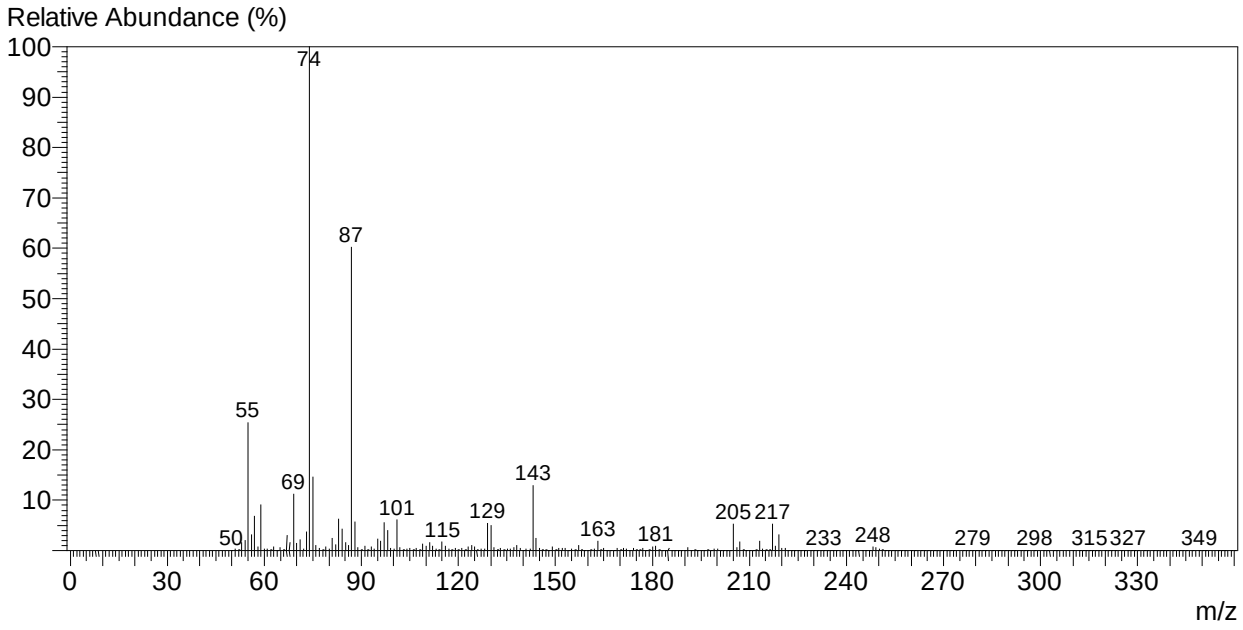

Figure 23. Electron-impact mass spectrum of 12-chlorododecanoic acid methyl ester (M+ = *m/z* 248)

Due to the complications in the FAME analysis, an alternative approach was needed. Derivatization of 12-bromododecanoic acid as its trimethylsilyl (TMS) ester was effected by reaction with *N*,*O*-bis(trimethylsilyl)trifluoroacetamide (BSTFA) containing 1% chlorotrimethylsilane. GC analysis revealed a single major peak at a retention time of 12.41 min (Figure 26). The mass spectrum of this species (Figure 27) showed a weak molecular ion at *m/z* 350 and 352 (0.2%), and the M−15 peaks corresponding to loss of methyl from the trimethylsilyl group. Other peaks were consistent with expectation for a TMS ester[48] notably the base peak at m/z 117, resulting from loss of methyl from *m/z* 132, the product of McClafferty rearrangement.

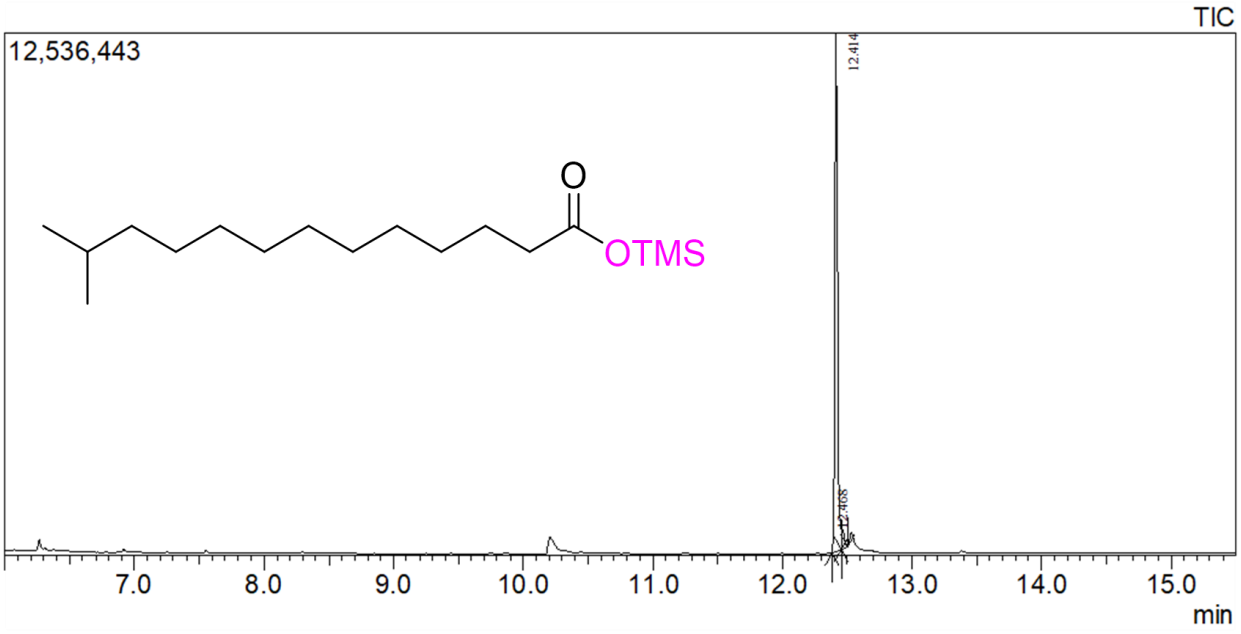

Figure 24. GC/MS total ion chromatogram of 12-bromododecanoic acid trimethylsilyl ester

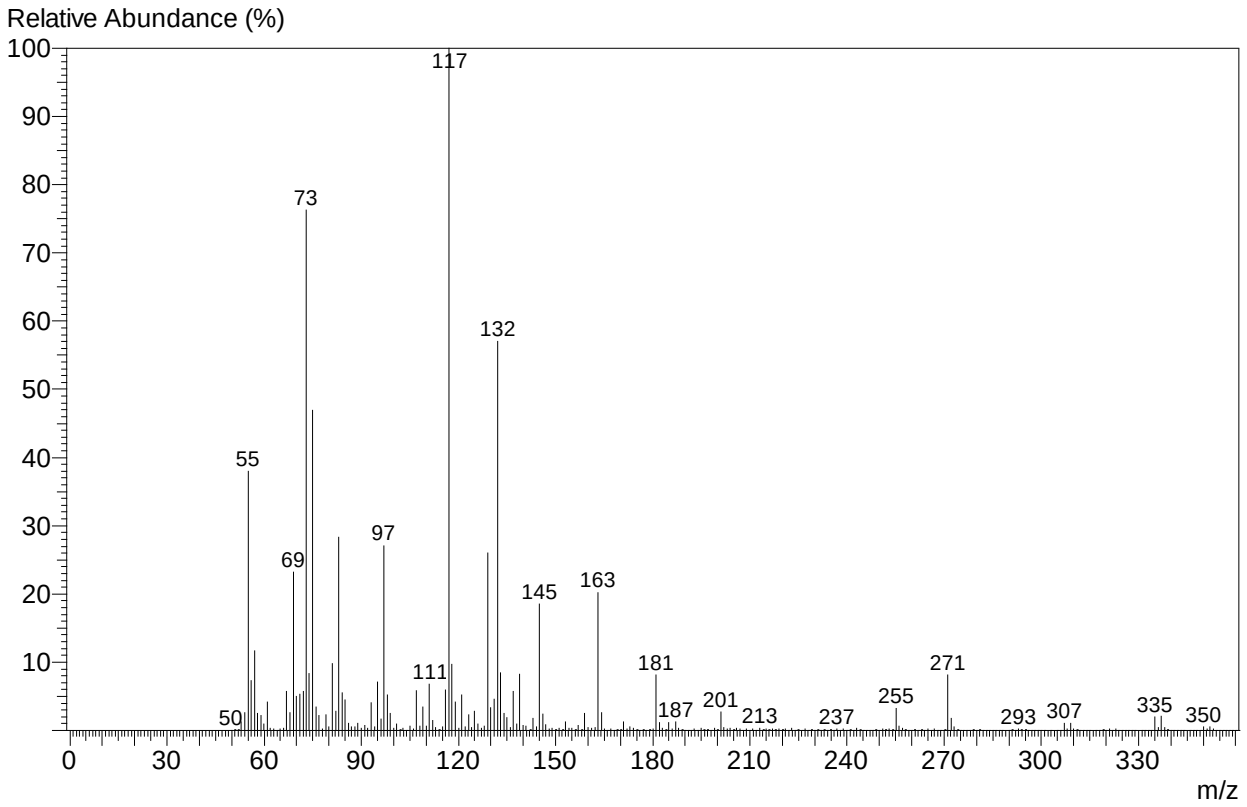

Figure 25. Electron-impact mass spectrum of 12-bromododecanoic acid trimethylsilyl ester (M+ = *m/z* 350)

Efforts Toward the Synthesis of Phosphatidylglycerol (PG) Lipids

Because bacterial PG lipids are unavailable commercially, we undertook a total synthesis, as outlined in Figure 28.[45] The phosphatidylglycerol unit was to be constructed as described by Lindberg and coworkers[45] starting from (*S*)-glycidol. Subsequently, the head-group glycerol would be attached stereospecifically starting from (*R*)-isopropylidene glycerol.[49] The first step was the synthesis of protected phosphoglyidol **3** by phosphorylation of commercially available (*S*)-glycidol using phosphoramidite **1** and 1H-tetrazole as a mild acid catalyst, producing an intermediate phosphite ester (Figure 29). The phosphite was then oxidized *in situ* with *m*-CPBA to produce the phosphate, which was purified by flash chromatography. ^{1}H NMR analysis (Figure 30) confirmed that the expected product had been obtained. According to Lindberg et al.,

the percentage yield for the synthesized phosphate ester was 74 %. The percentage yield for our synthesized phosphate ester after purification was about 10 %. The lower percentage yield of our synthesized phosphate ester might have resulted from slight differences in the procedure (especially the use of an acetonitrile solution of 1H-tetrazole rather than solid), insufficiently dry conditions, or greater losses during flash chromatography.

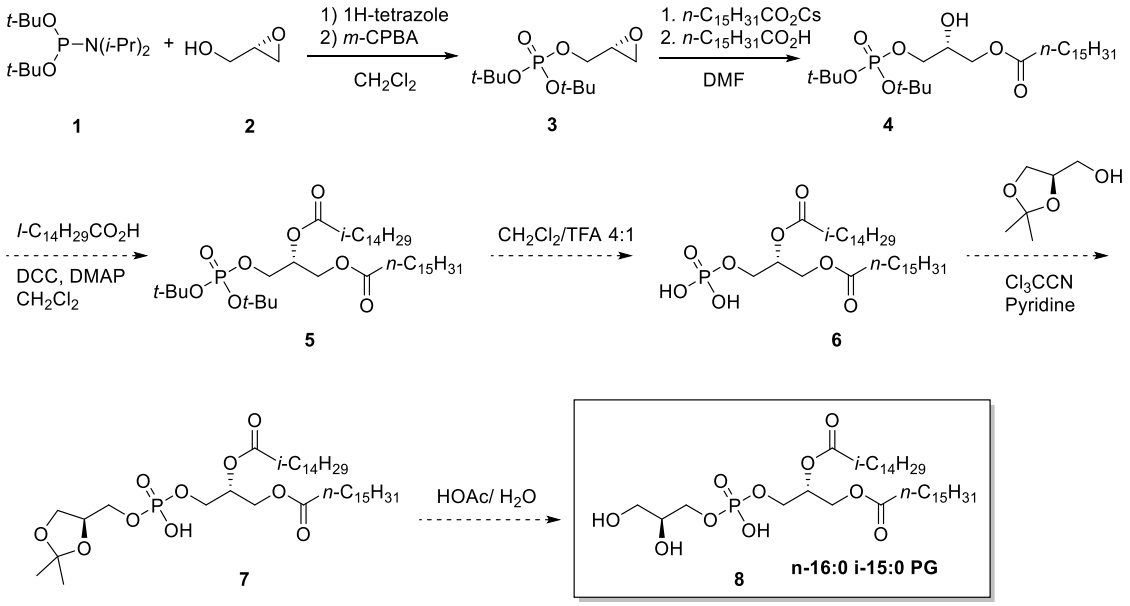

Figure 26. Proposed synthesis of phosphatidylglycerol. Solid arrows indicate completed steps, whereas dashed arrows are remaining steps

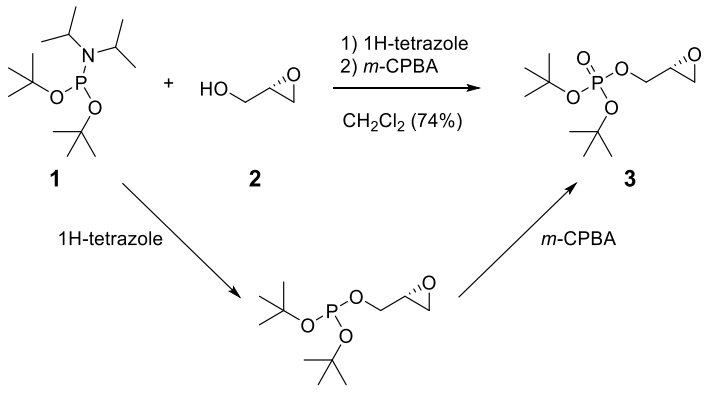

Figure 27. Synthesis of (*R*)-*O*-(di-*tert*-butylphosphono)glycidol **(3)**

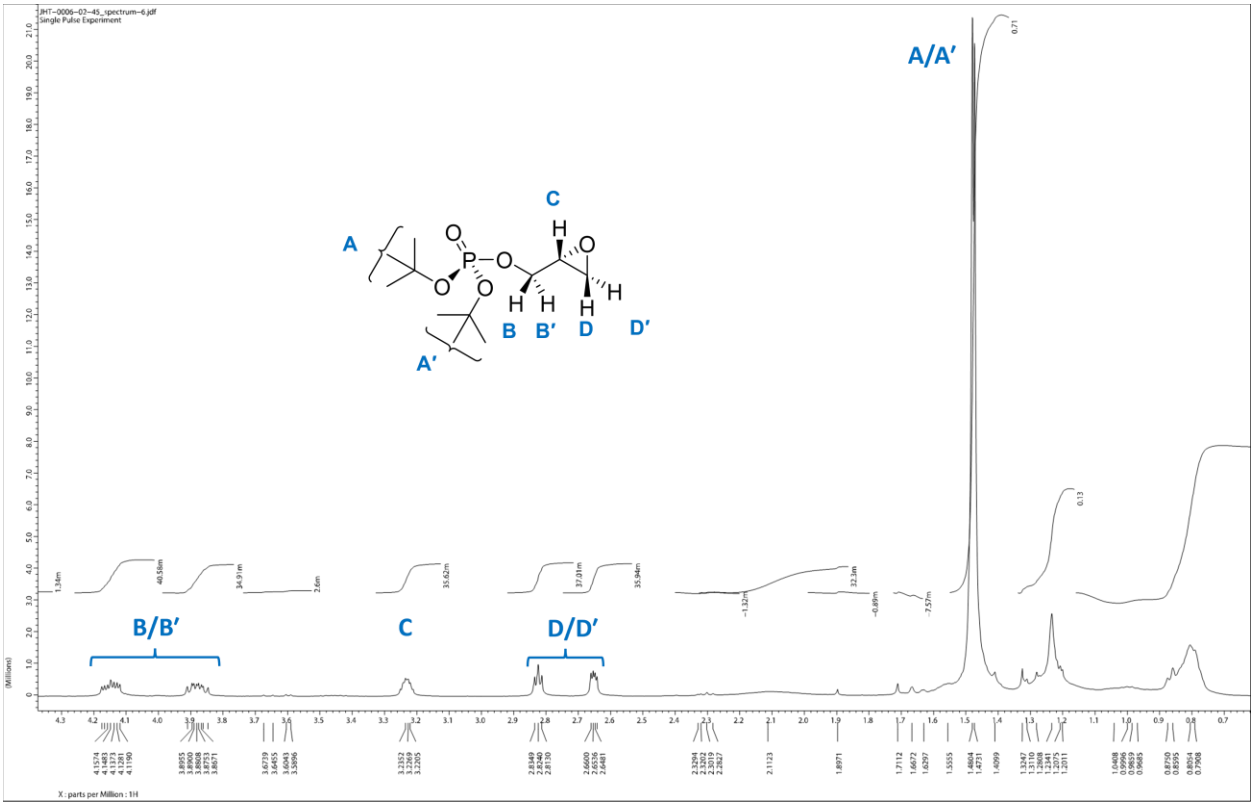

Figure 28. Partial ^{1}H NMR spectrum of phosphate ester **3**. The sets of diastereotopic protons A/A′, C/C′ and D/D′ are not specifically assigned.

The next step in the synthesis was installing the *sn*-1 acyl chain via nucleophilic opening of the epoxide. We chose palmitic acid (16:0, common in bacteria and eukaryotes) for the first model compound. For the reaction, palmitic acid was converted to its cesium salt by reaction of cesium carbonate with palmitic acid in methanol (Figure 31).

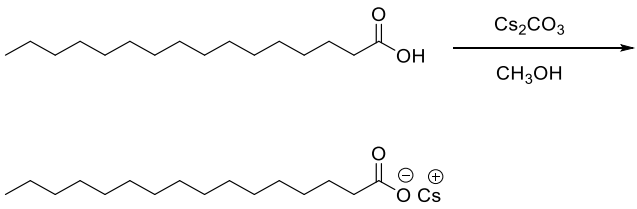

Figure 29. Synthesis of cesium palmitate

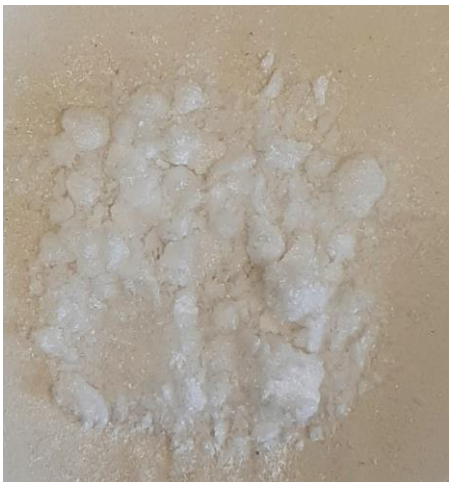

Figure 30. Cesium palmitate

The cesium palmitate and palmitic acid were then reacted with the epoxide in DMF at 80 °C as shown in Figure 33. Cesium palmitate regioselectively attacks the epoxide ring to introduce the palmitoyl group at the *sn*-1 position while leaving a free hydroxyl group with the correct stereochemistry at *sn*-2. The reaction proceeded cleanly, producing only the product 3-*O*-di-*tert*-butylphosphono-1-*O*-palmitoyl-*sn*-glycerol. Flash chromatography was used to remove unreacted cesium palmitate and palmitic acid. Lindberg et al. reported a yield of 74 %, whereas we obtained 53%. We expect that a higher yield could be obtained upon repetition of the procedure at larger scale.

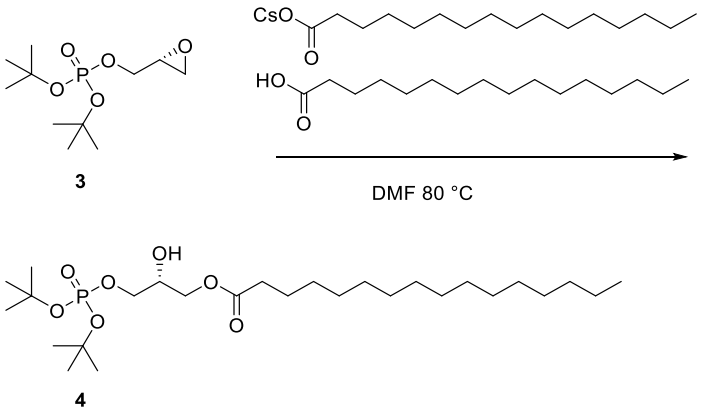

Figure 31. Epoxide ring opening

After purification, ^{1}H NMR spectroscopy was used for the characterization of the product. The ^{1}H NMR spectrum below (Figure 34) matched the data reported by Lindberg et al.

Time did not permit further elaboration of the PG lipids. The next planned steps are the subject of future work.

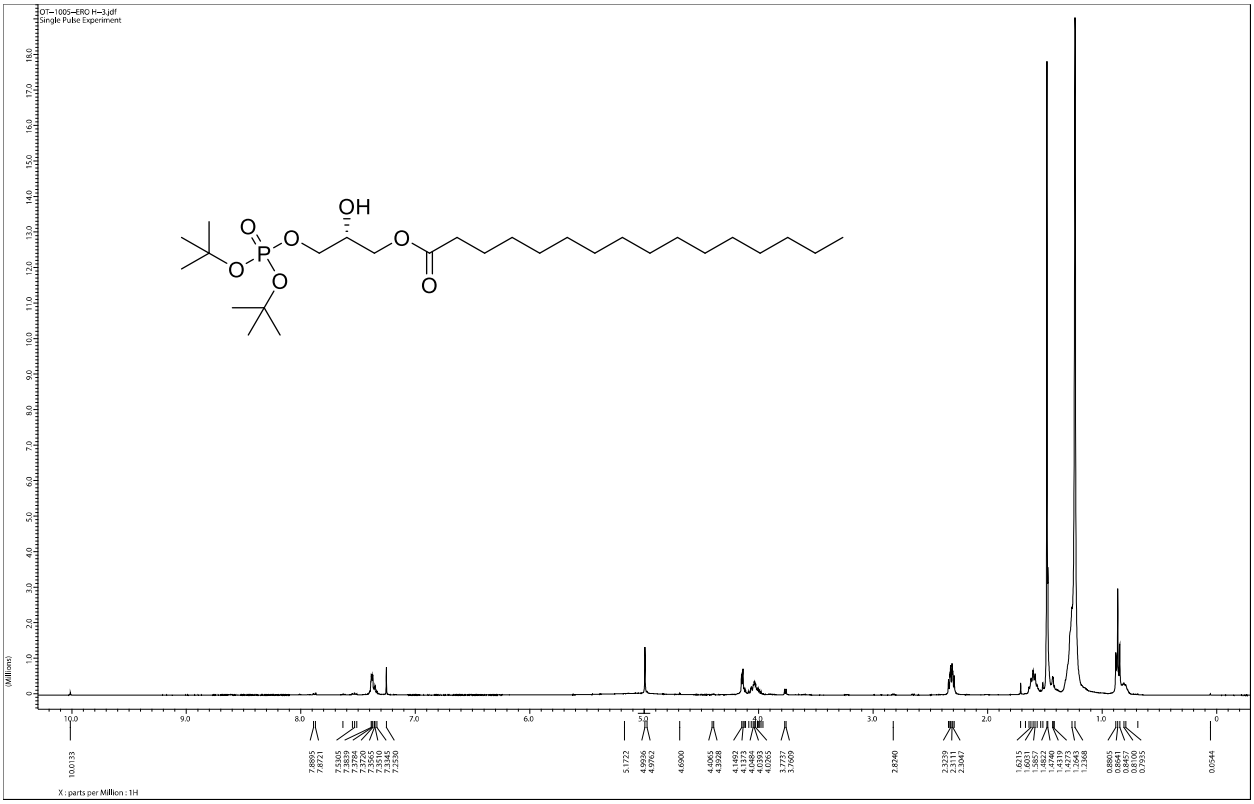

Figure 32. ^{1}H NMR spectrum of 3-*O*-di-*tert*-butylphosphoryl-1-*O*-palmitoyl-*sn*-glycerol **(4)**

Pilot Fluidity Measurements

Since fuel molecules are organic solvents that have disruptive effects on membranes, it is necessary to understand how these organic solvents disrupt the bacterial membrane. Insight can be gained through biophysical characterization of the membranes using fluorescence techniques.

These methods quantify physical properties like fluidity, which enables us to understand the how lipid structure and composition affects fuel tolerance.

As a prelude to studies with bacterial membrane models, fluidity experiments were performed using a commercially available mammalian PG lipid, POPG. This lipid was mixed with 0.2 mole percent Laurdan in chloroform/methanol, then evaporated to a dry film. The dried lipid/Laurdan mixture was rehydrated and formed into 100-nm unilamellar vesicles (UVs) by extrusion through a 100-nm pore-size membrane. Fluorescence emission spectra were recorded at several temperatures, and generalized polarization (GP) values were calculated. The two expected peaks at 440 and 490 nm were observed. It was further observed that the intensity of the 440-nm peak decreased relative to that of the 490-nm peak as the sample was heated from 20 ℃ to ~50 ℃ (Figure 35), resulting in a decrease in the GP value (Figure 36). From these experiments, we conclude that Laurdan is a promising probe for future studies of membrane fluidity.

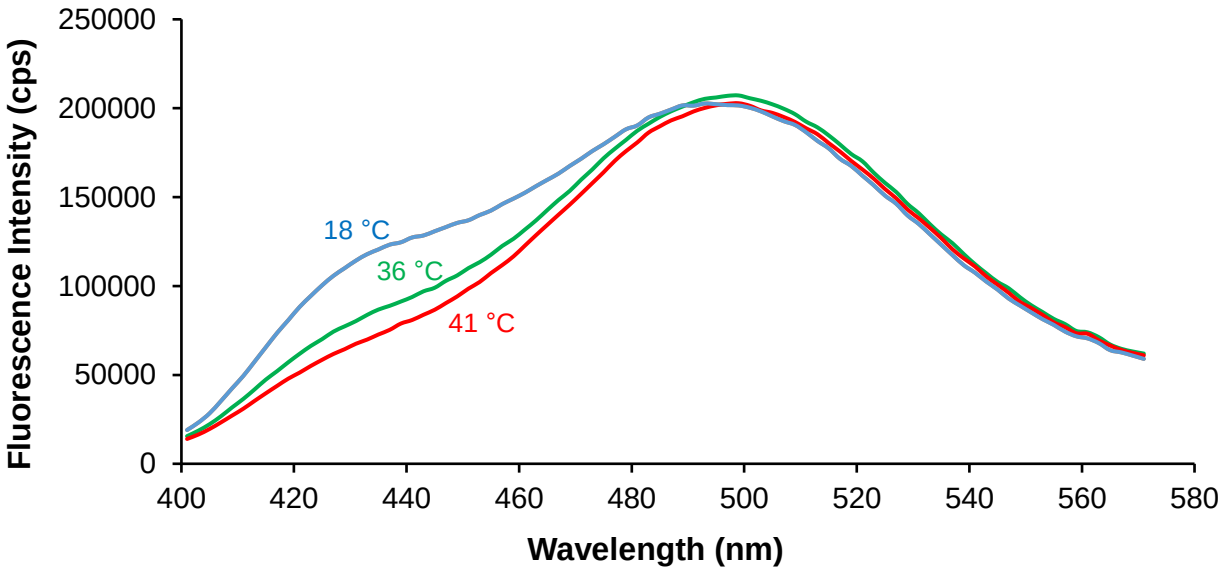

Figure 33. Temperature dependence of Laurdan fluorescence in POPG vesicles

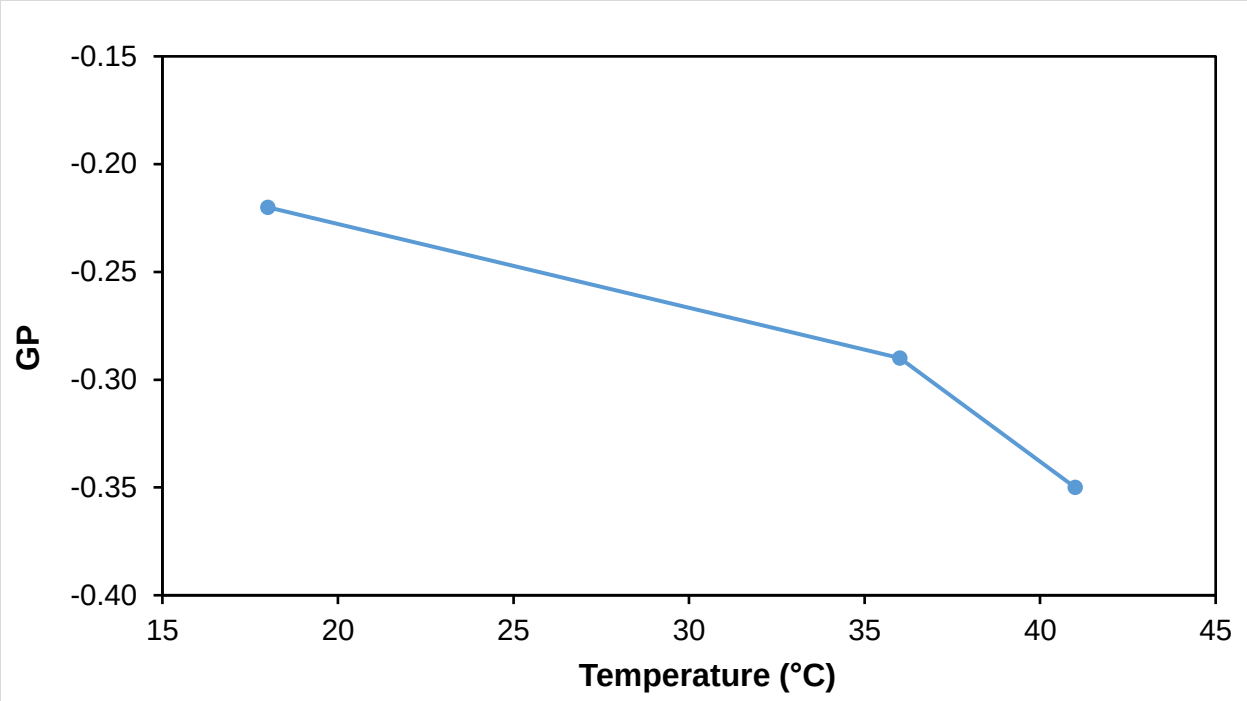

Figure 34. Laurdan general polarization vs. temperature in POPG vesicles

CHAPTER 4. CONCLUSION AND FUTURE WORK

In efforts toward the stereoselective synthesis of bacterial PG lipids, i-14:0 was synthesized and purified by vacuum distillation. Another acid, 12-bromododecanoic acid, was synthesized as the precursor for longer-chain (C_{17}) fatty acids. The compounds were characterized by GC/MS and ^{1}H NMR spectroscopy to establish identity and purity. Subsequently, a route toward the synthesis of PGs was designed, and the first steps completed. Specifically, (*S*)-glycidol was converted to a phosphoglycidol derivative with *t*-butyl protecting groups, then reacted with cesium palmitate to afford a protected lyso-phosphatidic acid. Finally, successful Laurdan general polarization measurements were made on a mammalian phosphatidylglycerol model, POPG, paving the way for future experiments with bacterial PG lipids and biofuels.

Future work would focus on attaching a series of branched fatty acid tails to the *sn*-2 position, deprotecting the phosphate moiety, coupling the resulting phosphatidic acids to isopropylidene glycerol, and deprotecting the glycerol side chain to afford PG lipids. The effects of biofuel-related molecules such as 1-butanol and THF would then be studied using Laurdan general polarization to judge effects on fluidity. Collaborative efforts to perform more detailed structural studies using X-ray and neutron scattering were also planned.

REFERENCES

1. Clifton, L. A., Campbell, R. A., Sebastiani, F., Campos-Terán, J., Gonzalez-Martinez, J. F., Björklund, S., Cárdenas, M. Design and use of model biomembranes to study biomolecular interactions using complementary surface-sensitive techniques. *Adv. Colloid Interface Sci*. **2020**, *227*, 102118. doi: 10.1016/j.cis.2020.102118.

2. Yin, H., Flynn, A. D. Drugging membrane protein interactions. *Annu. Rev. Biomed. Eng*., **2016**, *18*, 51–76. doi:10.1146/annurev-bioeng-092115-025322.

3. Overington, J. P., Al-Lazikani, B., & Hopkins, A. L. How many drug targets are there? *Nat. Rev. Drug Discovery*, **2006**, *5*, 993–996. doi:10.1038/nrd2199.

4. Sullivan, James A. CELLS alive https://www.cellsalive.com (accessed 08-15-2021)

5. Singer, S. J. The fluid mosaic model of membrane structure. In *Structure of Biological Membranes*; Abrahamsson, S., Pascher, I., Eds.; Nobel Foundation Symposia, Vol 34; Springer, 1977; pp 443–461. https://doi.org/10.1007/978-1-4684-8127-3_25.

6. Yèagle, P. L. Lipid regulation of cell membrane structure and function. *FASEB J*., **1989**, *3*, 1833–1842. https://doi.org/10.1096/fasebj.3.7.2469614.

7. Ansell, G. B., & Spanner, S. Chapter 1 Phosphatidylserine, phosphatidylethanolamine, and phosphatidylcholine. In *Phospholipids*; Hawthorne, J. N., Ansell G. B., Eds.; New Comprehensive Biochemistry**,** Vol. 4; Elsevier, 1982; pp 1–49. doi:10.1016/s0167-7306(08)60005-8.

8. Murzyn, K.; Róg, T.; Pasenkiewicz-Gierula, M. Phosphatidylethanolamine-phosphatidylglycerol bilayer as a model of the inner bacterial membrane. *Biophys. J.* **2005**, *88*, 1091–1103. https://doi.org/10.1529/biophysj.104.048835.

9. Lind, T. K.; Skoda, M. W. A.; Cárdenas, M. Formation and characterization of supported lipid bilayers composed of phosphatidylethanolamine and phosphatidylglycerol by vesicle fusion, a simple but relevant model for bacterial membranes. *ACS Omega*, **2019**, *4*, 10687–10694. https://doi.org/10.1021/acsomega.9b01075.

10. López, D., Vlamakis, H., & Kolter, R. Generation of multiple cell types in *Bacillus subtilis*. *FEMS Microbiol. Rev*., **2009**, *33*, 152–163. doi:10.1111/j.1574-6976.2008.00148.x

11. Kaneda, T. Fatty acids of the genus *Bacillus*: An example of branched chain preference. *Bacteriol. Rev*., **1977**, *41*, 391–418. https://doi.org/10.1128/mmbr.41.2.391-418.1977

12. Calder, P. C. Functional roles of fatty acids and their effects on human health. *JPEN, J. Parenter. Enteral Nutr*., **2015**, *39*, 18S–32S. doi:10.1177/0148607115595980

13. Burns, J. L., Nakamura, M. T., & Ma, D. W. L. Differentiating the biological effects of linoleic acid from arachidonic acid in health and disease. *Prostaglandins, Leukotrienes Essent. Fatty Acids*., **2018**, *135*, 1–4. doi:10.1016/j.plefa.2018.05.004

14. Assiesa J., Loka A., Bocktinga C. L, Weverlingb G. J., Lieversec R., Visserd I., Abelinge N. G. G. M., Durane M., and Schenea A. H. Fatty acids and homocysteine levels in patients with recurrent depression: an explorative pilot study. *Prostaglandins, Leukotrienes and Essent. Fatty Acids*, **2004**, *70*, 349–356. https://doi.org/10.1016/j.plefa.2003.12.009

15. Ristic V., and Ristic G. Role and importance of dietary polyunsaturated fatty acids in the prevention and therapy of atherosclerosis. *Med. Pregl*., **2003**, *56*, 50–53. https://doi.org/10.2298/mpns0302050r.

16. Šachl, R., Štěpánek, M., Procházka, K., Humpolíčková, J., & Hof, M. Fluorescence study of the solvation of fluorescent probes Prodan and Laurdan in poly(ε-caprolactone)-block-poly (ethylene oxide) vesicles in aqueous solutions with tetrahydrofurane. *Langmuir*, **2008**, *24*, 288–295. https://doi.org/10.1021/la702277t.

17 Norbert Kučerka, Mu-Ping Nieh, John Katsaras, Fluid phase lipid areas and bilayer thicknesses of commonly used phosphatidylcholines as a function of temperature, *Biochim. Biophys. Acta, Biomembr*. **2011**, *1808*, 2761–2771. https://doi.org/10.1016/j.bbamem.2011.07.022

18 Kučerka N, Tristram-Nagle S, Nagle JF. Structure of fully hydrated fluid phase lipid bilayers with monounsaturated chains. *J. Membr. Biol*. **2005**, *208*, 193–202. DOI: 10.1007/s00232-005-7006-8. PMID: 16604469

19. Sinensky, M. Homeoviscous adaptation—A homeostatic process that regulates the viscosity of membrane lipids in *Escherichia coli*. *Proc. Natl. Acad. Sci. U. S. A.*, **1974**, *71*, 522–525. doi:10.1073/pnas.71.2.522

20 Heipieper, H. J., Meinhardt, F., & Segura, A. The cis–trans isomerase of unsaturated fatty acids in *Pseudomonas* and *Vibrio*: Biochemistry, molecular biology and physiological function of a unique stress adaptive mechanism. *FEMS Microbiol. Lett*., **2003**, *229*, 1–7. doi:10.1016/s0378-1097(03)00792-4

21. Weber, G.; Farris, F. J. Synthesis and spectral properties of a hydrophobic fluorescent probe: 6-propionyl-2-(dimethylamino)naphthalene. *Biochemistry* **1979**, *18*, 3075–3078, DOI: 10.1021/bi00581a025

22. Sanchez, S. A.; Tricerri, M. A.; Gunther, G.; Gratton, E. Laurdan generalized polarization: From cuvette to microscope. In *Modern Research and Educational Topics in Microscopy*; Méndez-Vilas, A., Díaz, J., Eds.; Formatex, 2007; pp 1007–1014. doi.org/dx.doi.org/10.1.1.585.8626.

23. Lúcio, A.; Vequi-Suplicy, C.; Fernandez, R.; Lamy, M. T. Laurdan spectrum decomposition as a tool for the analysis of surface bilayer structure and polarity: A study with DMPG, peptides and cholesterol. *J. Fluoresc*., **2010**, *20*, 473–482. https://doi.org/10.1007/s10895-009-0569-5.

24. Barucha-Kraszewska, J., Kraszewski, S., & Ramseyer, C. Will C-Laurdan dethrone Laurdan in fluorescent solvent relaxation techniques for lipid membrane studies?, *Langmuir*, **2013**, *29*, 1174–1182. doi:10.1021/la304235r.

25. Bacalum, M., Zorilă, B., & Radu, M. Fluorescence spectra decomposition by asymmetric functions: Laurdan spectrum revisited. *Anal. Biochem*., **2013**, *440*, 123–129. doi:10.1016/j.ab.2013.05.031.

26. Golfetto O., Hinde E., Gratton E. The Laurdan spectral phasor method to explore membrane micro-heterogeneity and lipid domains in live cells. In *Methods in Membrane Lipids*; Owen D., Ed.; Methods in Molecular Biology (Methods and Protocols), Vol. 1232; Humana Press, 2015; pp 273–290. https://doi.org/10.1007/978-1-4939-1752-5_19.

27. Vequi-Suplicy, C. C., Coutinho, K., & Lamy, M. T. New insights on the fluorescent emission spectra of Prodan and Laurdan. *J. Fluoresc*., **2015**, *25*, 621–629. doi:10.1007/s10895-015-1545-x.

28. Malacrida, L., Astrada, S., Briva, A., Bollati-Fogolín, M., Gratton, E., & Bagatolli, L. A. Spectral phasor analysis of Laurdan fluorescence in live A549 lung cells to study the hydration and time evolution of intracellular lamellar body-like structures. *Biochim. Biophys. Acta, Biomembr*., **2016**, *1858*, 2625–2635. Doi: 10.1016/j.bbamem.2016.07.017.

29. Tiziana Parasassi; Ewa K. Krasnowska; Luis Bagatolli; Enrico Gratton. Laurdan and Prodan as polarity-sensitive fluorescent membrane probes. *J. Fluoresc*. **1998**, *8*, 365–373. doi:10.1023/a:1020528716621

30. Harris, F. M.; Best, K. B.; Bell, J. D. Use of Laurdan fluorescence intensity and polarization to distinguish between changes in membrane fluidity and phospholipid order. *Biochim. Biophys. Acta, Biomembr*. **2002**, *1565*, 123–128. https://doi.org/10.1016/S0005-2736(02)00514-X

31. Bartholomew, J. W., & Mittwer, T. cell structure in relation to the Gram reaction as shown during lysis of *Bacillus subtilis*. *J. Gen. Microbiol*., **1951**, *5*, 39–45. doi:10.1099/00221287-5-1-39

32. Bacterial spore formers: probiotics and emerging applications; Ricca, E., Henriques, A. O., Cutting, S. M., Eds.; Horizon Bioscience, 2004; pp 20–59.

33. Merrill, L., Dunbar, J., Richardson, J., & Kuske, C. R. Composition of *Bacillus* species in aerosols from 11 U.S. cities. *J. Forensic Sci*., **2006**, *51*, 559–565. doi:10.1111/j.1556-4029.2006.00132. x.

34. Kovács, Á. T. *Bacillus subtilis*. *Trends Microbiol*., **2019**, *27*, 724–725. https://doi.org/10.1016/j.tim.2019.03.008.

35. Jaenicke, R. Abundance of cellular material and proteins in the atmosphere. *Science* **2005**, *308*, 73–73. doi:10.1126/science.1106335.

36. Simons, K., & Vaz, W. L. C. Model systems, lipid rafts, and cell membranes. *Annu. Rev. Biophys. Biomol. Struct*., **2004**, *33*, 269–295. https://doi.org/10.1146/annurev.biophys.32.110601.141803.

37. Harwood, C. R. *Bacillus subtilis* and its relatives: molecular biological and industrial workhorses. *Trends Biotechnol*., **1992**, *10*, 247–256. doi.org/10.1016/0167-7799(92)90233-L.

38. Nickels, J. D.; Chatterjee, S.; Stanley, C. B.; Qian, S.; Cheng, X.; Myles, D. A. A.; Standaert, R. F.; Elkins, J. G.; Katsaras, J. The in vivo structure of biological membranes and evidence for lipid domains. *PLOS Biol*. **2017**, *15*, e2002214. https://doi.org/10.1371/journal.pbio.2002214

39. Peralta-Yahya, P. P., & Keasling, J. D. Advanced biofuel production in microbes. *Biotechnol. J*., **2010**, *5*, 147–162. https://doi.org/10.1002/biot.200900220.

40 Smith, M. D.; Pingali, S. V.; Elkins, J. G.; Bolmatov, D.; Standaert, R. F.; Nickels, J. D.; Urban, V. S.; Katsaras, J.; Davison, B. H.; Smith, J. C.; Petridis, L. Solvent-induced membrane stress in biofuel production: molecular insights from small-angle scattering and all-atom molecular dynamics simulations. *Green Chem*., **2020**, *22*, 8278–8288. https://doi.org/10.1039/D0GC01865A.

41. Bamdad, H., Hawboldt, K., & MacQuarrie, S. A review on common adsorbents for acid gases removal: Focus on biochar. *Renewable Sustainable Energy Rev*., **2018**, *81*, 1705–1720. doi: 10.1016/j.rser.2017.05.261

42. Heipieper, H. J., Weber, F. J., Sikkema, J., Keweloh, H., & de Bont, J. A. M. Mechanisms of resistance of whole cells to toxic organic solvents. *Trends Biotechnol*., **1994**, *12*, 409–415. https://doi.org/10.1016/0167-7799(94)90029-9.

43. Baer T. A.; Carney, R,. L. Carney. Copper catalyzed reaction of Grignard reagents with chloromagnesium salts of ω-bromoacids. , **1976**, *17*, 4697–4700. doi:10.1016/s0040-4039(00)92999-x

44. Bidd, I., Kelly, D. J., Ottley, P. M., Paynter, O. I., Simmonds, D. J. & Whiting, M. C. Convenient syntheses of bifunctional C_{12}-acyclic compounds from cyclododecanone. *J. Chem. Soc., Perkin Trans. 1*, **1983**, 1369–1372. https://doi.org/10.1039/P19830001369

45. Lindberg, J., Ekeroth, J., & Konradsson, P. Efficient synthesis of phospholipids from glycidyl phosphates. *J. Org. Chem*., **2002**, *67*, 194–199. https://doi.org/10.1021/jo010734+.

46. Kruizinga, W. H., Strijtveen, B., & Kellogg, R. M. Cesium carboxylates in dimethyl formamide. Reagents for introduction of hydroxyl groups by nucleophilic substitution and for inversion of configuration of secondary alcohols. *J. Org. Chem*., **1981**, *46*, 4321–4323. doi:10.1021/jo00334a05

47. Malacrida, L., Jameson, D. M., & Gratton, E. A multidimensional phasor approach reveals Laurdan photophysics in NIH-3T3 cell membranes. *Sci. Rep*., **2017**, *7*, 9215. doi:10.1038/s41598-017-08564-z

48 Tulloch, A. P. Mass spectra of TMS esters of deuterated decanoic acids and of TMS ethers of deuterated decanols. *Lipids*, **1985**, *20*, 404–411. https://doi.org/10.1007/BF02534230

49. Gagnon, M. C.; Dautrey, S.; Bertrand, X.; Auger, M.; Paquin, J. F. A flexible synthetic approach to phosphatidylglycerols. *Eur. J. Org. Chem*. **2017**, *2017*, 6401–6407. https://doi.org/10.1002/ejoc.201701178.

VITA

ENOCH AGANGLORO ASIMBISA

Education: BSc. Chemistry, Kwame Nkrumah University of Science and Technology, Kumasi, Ghana, 2018

MS Chemistry, East Tennessee State University, Johnson City, Tennessee, 2021

Professional Experience: Assistant to Dean of Students, Kwame Nkrumah University of Science and Technology; Kumasi, Ghana, 2019

Graduate Assistant, Department of Chemistry, College of Arts and Sciences, East Tennessee State University, 2019– 2021